Chapter 6
Removal of Antibiotics from Water by Adsorption/Biosorption on Adsorbents from Different Raw Materials

José Rivera-Utrilla, Manuel Sánchez-Polo, and Raúl Ocampo-Pérez

Abstract The present chapter aimed to analyze and compare the behavior of carbon materials, both commercial (activated carbons) and prepared in our laboratories (sludge-derived materials and activated carbons from petroleum coke) with different chemical and textural characteristics in the adsorption of tetracyclines and nitroimidazoles from water. This behavior was analyzed in both static and dynamic regimes and using ultrapure water, surface water, groundwater, and urban wastewater. We also assessed the influence of the solution chemical nature (pH and ionic strength) on the adsorption of these pharmaceutical contaminants analyzing the adsorbent-adsorbate interaction types and evaluating the effectiveness of the combined use of microorganisms and activated carbon (bioadsorption) in these adsorption processes. Additionally, the mass transport mechanisms controlling the overall adsorption rate of these adsorbate-adsorbent systems were investigated in depth, and relationships between textural and chemical characteristics of these adsorbent materials with kinetic and diffusion parameters were reported.

Keywords Adsorption • Carbon materials • Tetracyclines • Nitroimidazoles

Contents

J. Rivera-Utrilla (✉) • M. Sánchez-Polo
Inorganic Chemistry Department, University of Granada, 18071, Granada, Spain
e-mail: jrivera@ugr.es; mansanch@ugr.es

R. Ocampo-Pérez
Center of Research and Postgraduate Studies, Faculty of Chemical Science, Autonomous University of San Luis Potosí, Av. Dr. M. Nava No. 6, San Luis Potosí, SLP 78210, Mexico
e-mail: ocampor@uaslp.mx

A. Bonilla-Petriciolet et al. (eds.), *Adsorption Processes for Water Treatment and Purification*, DOI 10.1007/978-3-319-58136-1_6

6.1 Introduction

A constant flow of new products is generating novel contaminants with unknown short-, medium-, or long-term effects on the environment and human health that are not governed by regulations on the maximum allowable concentrations in the environment (Halling-Sørensen et al. 1998; Calamari 2002; Adler et al. 2008; Cooper et al. 2008; Rivera-Utrilla et al. 2013b). They include chemical compounds in cosmetics (creams, perfumes, makeup), domestic products (degreasants, glass cleaners, detergents), and pharmaceuticals, which are causing the greatest concern due to their very wide variety and elevated consumption (Adler et al. 2008; Cooper et al. 2008; Rivera-Utrilla et al. 2013b). For example, over 3000 different pharmaceutical substances are used in the UK (Ayscough et al. 2000), and the annual production for human consumption in the European Union is estimated to exceed 100 tons per member country (Kümmerer 2008). Antibiotics are the most heavily used medical drugs in the European Union, with an estimated annual consumption of around 10,000 tons (Kümmerer 2008). It should also be noted that these consumption figures are considerably increased by the use of many of these products in veterinary medicine. After administration, large amounts of antibiotics and their byproducts are discharged into municipal wastewater that high concentrations of antibiotics are now detected in waters intended for human consumption, reducing their quality. They generally have a low biodegradability (Al-Ahmad et al. 1999; Kümmerer et al. 2000) and high toxicity (Kümmerer 2001), and some are reported to have mutagenic and carcinogenic characteristics (Bendesky et al. 2002).

Some of the most important antibiotic groups, tetracyclines (TCs) and nitroimidazoles, have been detected in waters (Halling-Sørensen et al. 1998; Calamari 2002; Rivera-Utrilla et al. 2013b). The TCs are bacteriostatic agents that act by inhibiting bacterial protein synthesis. They show activity against a wide variety of microorganisms and are used as antibiotics in humans and animals (Mathers et al. 2011; Gao et al. 2012b). Due to their low cost, TCs are also used as a food additive to enhance the growth rate of animals, adding a further pathway for their entry into the environment alongside emissions from the manufacture and formulation of the compounds and the disposal of unused or expired products. In surface waters, TCs

were detected at concentrations ranging from 0.11 to 4.20 μg/L (Lin et al. 2009), while concentrations in an effluent of a wastewater treatment plant ranged from 46 to 1300 ng/L for tetracycline, 270 to 970 ng/L for chlortetracycline, and 240 ng/L for oxytetracycline (Ternes et al. 2002; Yang et al. 2005; Batt et al. 2007; Stackelberg et al. 2007; Lin et al. 2009; Gao et al. 2012b). On the other hand, nitroimidazole antibiotics are widely used to treat infections caused by anaerobic and protozoan bacteria (e.g., *Trichomonas vaginalis* and Giardia lamblia) in humans and animals and are added to chow for fish and fowl (Tally et al. 1981; Lau et al. 1992; Lindberg et al. 2004), leading to their accumulation in animals, fish farm waters, and, especially, meat industry effluents (Kümmerer 2001). Nitroimidazoles have also been detected in waters at concentrations of 0.1–90.2 μg/L (Lindberg et al. 2004). Importantly, the presence of traces of TCs and nitroimidazoles in the environment can lead to the appearance of microorganisms that are resistant to these antibiotics and to which humans may be exposed via drinking water (Stackelberg et al. 2007).

Nowadays, studies have demonstrated that conventional treatment plants, mainly based on the use of microorganisms, have proven inadequate to effectively remove antibiotics from water, largely due to their complex molecular structure (Kümmerer et al. 2000; Carballa et al. 2004; Rivera-Utrilla et al. 2013b). Thus, the US Environmental Protection Agency recommended the adsorption on activated carbon as the best available technology for removing nonbiodegradable toxic organic compounds from drinking water and industrial wastewater (USEPA 1991).

Both granular (GAC) and powdered (PAC) activated carbons have been widely used for the adsorption of organic micropollutants in solution due to their chemical and textural properties (Radovic et al. 2001; Moreno-Castilla 2004; Dias et al. 2007; Rivera-Utrilla et al. 2011; Beita-Sandí et al. 2016). The capacity of activated carbon to adsorb pharmaceutical-related pollutants has attracted research interest (Snyder et al. 2007; Choi et al. 2008; Simazaki et al. 2008; Yu et al. 2008; Calisto et al. 2015; Zhu et al. 2015; Vidal et al. 2015). Besides, an important advantage of using activated carbon to remove pharmaceuticals is that toxic or pharmacologically active products are not generated.

Snyder et al. (2007) assessed the mechanisms underlying the adsorption of various pharmaceuticals and hormones on GAC and PAC and obtained removal percentages of around 90% for most of the pharmaceuticals studied. Optimal performances were obtained for acetaminophen (73–84%), carbamazepine (74–86%), triclosan (90–96%), and fluoxetine (91%), but the removal percentage did not exceed 50% for naproxen, diclofenac, gemfibrozil, sulfamethoxazole, and ibuprofen, among other drugs. They observed that the effectiveness of activated carbon was markedly reduced in the presence of natural organic matter (NOM), which competes for the active sites on the carbon, blocking its porosity.

Various authors have studied the adsorption of tetracyclines using adsorbents other than carbon, including apatites (Misra 1991), clays, and soils (Figueroa et al. 2004; Kulshrestha et al. 2004; Jones et al. 2005; Başakçilardan-Kabakci et al. 2007; Turku et al. 2007; Gu and Karthikeyan 2008; Parolo et al. 2008; Chang et al. 2012). Thus, Jones et al. (2005) evidenced that the iron oxide content, cation exchange

capacity, and soil texture have high influence on the sorption of TCs on soils with organic carbon content between 0% and 4%. Parolo et al. (2008) investigated the removal of tetracycline on montmorillonite as a function of pH and ionic strength. The results revealed that tetracycline can intercalate into the interlayer space of montmorillonite. Additionally, at pH 4, the highest tetracycline removal is obtained because, at this pH, tetracycline is in cationic form favoring the cation exchange. Finally, the presence of sodium ions reduces the adsorption capacity of montmorillonite.

TCs can be also removed from aqueous solutions by adsorption on different carbon materials such as $MnFe_2O_4$/activated carbon composites (Shao et al. 2012), graphene oxide (Gao et al. 2012a), and multiwalled carbon nanotubes (Zhang et al. 2011). However, fewer data are available on activated carbon as TC adsorbent. Choi et al. (2008) found activated carbon columns to be highly effective for the adsorption of seven TCs in aqueous medium, obtaining percentage removal values of around 90% that varied according to the type of TC and characteristics of the water, especially the concentration of NOM. They reported a higher adsorption capacity of activated carbon for TCs than for sulfonamide, despite the greater hydrophobicity of the latter.

In reference to nitroimidazole adsorption, Carrales-Alvarado et al. (2014) investigated the removal of MNZ on novel carbon materials with different chemical and textural characteristics. It was found that the chemical and textural characteristics of carbon adsorbents play a key role in the adsorption of MNZ in aqueous solution. Carbon materials with a large surface area and low content of carboxylic groups are preferable for the removal of nitroimidazoles from aqueous solution. Carbon materials can be effectively applied to remove MNZ from wastewater, because the adsorption of electrolytes in the water cooperates rather than competes with its adsorption. Additionally, the adsorption of MNZ on carbon materials is reversible, allowing the exhausted adsorbents to be regenerated by contacting them with water. Adsorption kinetic data published by Ahmed and Theydan (2013) showed that the adsorption rate of metronidazole (MNZ) on activated carbon from an agricultural waste follows a pseudo-second-order model, and estimation of the heat of adsorption revealed that the adsorption of MNZ was endothermic.

In order to further deepen in the interactions established in the adsorption of tetracyclines and nitroimidazole drugs on different adsorbent materials, the present chapter aimed to outline results obtained during the development of a wider project to analyze and compare the behavior of carbon materials, both commercial (activated carbons) and prepared in our laboratories (sludge-derived materials and activated carbons from petroleum coke) with different chemical and textural natures in the adsorption of tetracyclines and nitroimidazoles from water. This behavior was analyzed in both static and dynamic regime and using ultrapure water, surface water, groundwater, and urban wastewater. We also assessed the influence of solution chemical nature (pH and ionic strength) on the adsorption of these compounds analyzing the adsorbent-adsorbate interaction types and evaluated the combined use of microorganisms and activated carbon (biosorption) in these adsorption processes. Besides, the design of an adsorption system to treat

wastewater also requires data on the adsorbate concentration decay curves of the adsorbate/adsorbent system and on the mechanisms controlling the adsorption kinetics. Therefore, other objectives of this project were (i) to apply diffusional and kinetic models to explain the overall adsorption rate of both tetracyclines and nitroimidazoles on the adsorbents selected, (ii) to investigate the mass transport mechanism controlling the overall adsorption rate, and (iii) to analyze the relationship of textural and chemical characteristics of these adsorbent materials with kinetic and diffusion parameters.

The first part of this chapter is concerned with the chemical and textural characterization of the adsorbents to remove TCs and nitroimidazoles from water. The preparation methods of both sludge-derived materials and activated carbons from petroleum coke will be also analyzed. The particular objective of this part was to optimize adsorbent material preparation by means of a statistical experimental planning method, obtaining materials derived from sludge and petroleum coke by chemical activation with NaOH and KOH, respectively, at high temperatures and establishing the properties required for the removal of contaminants from water. Special attention was paid to the effect of binders on the surface and adsorbent characteristics of these new materials. Some of the results obtained in this wider project have already been published (Sánchez-Polo and Rivera-Utrilla 2006; Rivera-Utrilla et al. 2009; Méndez-Díaz et al. 2010; Gómez-Pacheco et al. 2012; Ocampo-Pérez et al. 2012; Ocampo-Pérez et al. 2013; Rivera-Utrilla et al. 2013a; Ocampo-Pérez et al. 2015). This chapter summarizes these findings.

6.2 Adsorbent Materials

The adsorbents used in this study were commercial activated carbons, sludge-derived materials, and activated carbons from petroleum coke. All adsorbents were characterized by determining their surface area, pore volume accessible to water, pore size distribution, oxygen surface groups, and pH of the point of zero charge (pH_{PZC}). Sludge-derived materials were also characterized by X-ray fluorescence and chemical and elemental analyses.

6.2.1 Commercial Activated Carbons

Sorbo (S) and Merck (M) commercial activated carbons, with a particle diameter ranging between 0.6 and 1 mm were used in this study. The experimental methods followed to characterize the adsorbents were described in detail elsewhere (Sánchez-Polo and Rivera-Utrilla 2003; Rivera-Utrilla and Sánchez-Polo 2004; Bautista-Toledo et al. 2008; Gómez-Pacheco et al. 2012). Table 6.1 depicts the textural characteristics of activated carbons used in this study: both of them have a large surface area ($>1200\ m^2/g$) and a highly developed microporosity. Micropore

Table 6.1 Textural characteristics of commercial activated carbons

Activated carbon	S_{BET}[a] (m^2/g)	$W_o(N_2)$[b] (cm^3/g)	$W_o(CO_2)$[c] (cm^3/g)	$L_o(N_2)$[d] (nm)	$L_o(CO_2)$[e] (nm)	S_{ext}[f] (m^2/g)	V_2[g] (cm^3/g)	V_3[h] (cm^3/g)
S	1225	0.39	0.29	1.02	0.70	46.90	0.04	0.48
M	1301	0.42	0.29	1.69	0.70	41.90	0.10	0.28

[a]Surface area determined from N_2 adsorption isotherms at 77 K
[b,c]Volumes of micropores determined by N_2 and CO_2 adsorption, respectively
[d,e]Mean widths of micropores determined with the Dubinin equation
[f]External surface area determined by mercury porosimetry
[g]Volume of pores with diameter of 6.6–50 nm determined by mercury porosimetry
[h]Volume of pores with diameter >50 nm determined by mercury porosimetry

Table 6.2 Chemical characteristics of the commercial activated carbons

Activated carbon	Carboxylic groups (meq/g)	Carbonyl groups (meq/g)	Acidic groups (meq/g)	Basic groups (meq/g)	pH_{PZC}
S	0.00	0.15	0.45	1.08	9.0
M	0.04	0.84	0.40	0.44	7.7

volumes, deduced from N_2 adsorption, were considerably higher than those from CO_2 adsorption (Table 6.1), indicating a very heterogeneous micropore distribution in the activated carbon. Because CO_2 is only adsorbed in smaller size micropores (ultramicropores), whereas N_2 is adsorbed on the surface of all micropores (Garrido et al. 1987; Rodriguez-Reinoso and Linares-Solano 1989), N_2 adsorption data yield the total micropore volume, $W_0(N_2)$. Thus, the mean micropore size (L_0) was higher when determined by N_2 versus CO_2 adsorption (Table 6.1).

Table 6.2 lists the chemical characteristics of both activated carbons, showing that they are predominantly basic, with pH of point of zero charge values of 7.7 (carbon M) and 9.0 (carbon S).

6.2.2 Sludge-Derived Materials

Environmental concerns have been raised about the management of the sludge remaining after the primary and secondary treatment of urban wastewaters (Werther and Ogada 1999). It is a semisolid slurry with a content of little economic value and can have a major impact on the environment. Sludge, which is a subproduct of most wastewater treatment processes, is considered dangerous toxic waste and is generally used as fertilizer (Campbell 2000; Oleszkiewicz and Mavinic 2001). Sludge has conventionally been removed to monofills or sanitary landfills, but alternative options have been proposed. One of these is to incorporate sludge into the soil after its stabilization, e.g., by composting techniques; taking advantage of its high content in organic matter, phosphorus, nitrogen, and

potassium, among others; and enabling its utilization in the recovery of eroded land (Passuello et al. 2012). In this investigation, treatment plant sludge was used to prepare materials with the appropriate chemical and textural properties for the adsorption of organic and inorganic compounds.

6.2.2.1 Preparation of Adsorbent Materials from Sludge

The adsorbent materials were obtained from treatment plant sludge supplied by *Aguas y Servicios de la Costa Tropical de Granada (Spain)*. Sludge was transformed into adsorbent materials by thermal pyrolysis and chemical activation. It was chemically activated with sodium hydroxide by sludge impregnation, mixing the precursor with a solution of NaOH and binding agent (humic matter, phenolic resins, or clayey soil). After impregnation, the sample was left to dry under infrared lamps for approximately 12 h. The proportion of NaOH ranged from 5 to 100 g/100 g of sample and the proportion of binder from 0 to 20 g/100 g. After drying, the sample underwent pyrolysis in a model RO 10/100 Heraeus tubular oven equipped with Jumo-Digimat temperature programmer under controlled N_2 atmosphere (99.998%) with flow of 5 L/min, from 300 °C to 700 °C (ramps of 10 °C/min), maintaining the maximum temperature for periods ranging from 30 min to 3 h. The yield obtained in the preparation of these adsorbent materials was around 30%.

The binders or agglutinants selected were humic acid (Sigma Aldrich), clayey soil, and phenolic resins (both Ismael Quesada Chemical products). Humic acid was selected for its high carbon content and its utilization in briquetting processes, clayey soil for its binding capacity and low cost, and phenolic resins due to reports on their ability to bind different types of particles (Cavdar et al. 2008; Benk 2010; Correa et al. 2010; Wang et al. 2011). Table 6.3 lists the designations of the prepared samples.

6.2.2.2 Optimization of Sludge Activation Process

Optimization of Sludge Activation Process Without Binder (Linear Model)

Multivariate analyses were performed to optimize the sludge activation process, using a mathematical and statistical methodology that permits optimal planning of the experiment sequence, minimizing the cost of the experiment and the influence of experimental error (Hunter and Hunter 1978). The MODDE 7.0 statistical program was used for the experimental design and to optimize the preparation of adsorbent materials from treatment plant sludge.

The experimental conditions were varied in order to determine the optimal NaOH dose, pyrolysis temperature, and pyrolysis time for obtaining adsorbent materials with maximum tetracycline adsorption capacity. This effect was visualized by using a linear scanning model to study the response surface, conducting 11 experiments and varying the following factors: (A) amount of NaOH (from 5 to

Table 6.3 Designations assigned to the adsorbent samples prepared from biological treatment plant sludge (Gómez-Pacheco et al. 2012)

Experimental conditions						
Sample name	T (°C)	Type of binder	Binder (g)	NaOH (g)	Pyrolysis time (h)	Response q_e (mg/L)
CL	700	–	–	–	3.0	–
C1′	300	–	–	5.0	0.5	–
C2′	300	–	–	100.0	0.5	–
C3′	700	–	–	5.0	0.5	100
C4′	700	–	–	100.0	0.5	300
C5′	300	–	–	5.0	3.0	–
C6′	300	–	–	100.0	3.0	10
C7′	700	–	–	5.0	3.0	400
C8′	700	–	–	100.0	3.0	560
C9′	500	–	–	52.5	1.8	200
C10′	500	–	–	52.5	1.8	210
C11′	500	–	–	52.5	1.8	205
C2	700	–	–	50.0	3.0	–
C3	700	Humic ac.	10.0	25.0	3.0	418.3
C4	700	Humic ac.	10.0	50.0	3.0	466.6
C5	700	Humic ac.	20.0	25.0	3.0	406.8
C6	700	Humic ac.	0.0	25.0	3.0	407.5
C8	550	Humic ac.	10.5	30.0	2.0	352.4
C9	700	Humic ac.	20.0	50.0	3.0	415.9
C10	400	Humic ac.	20.0	50.0	3.0	–
C11	400	Humic ac.	20.0	50.0	1.0	–
C12	700	Humic ac.	20.0	10.0	3.0	242.9
C13	700	Humic ac.	1.0	10.0	1.0	278.4
C15	700	Humic ac.	20.0	10.0	1.0	219.7
C16	700	Humic ac.	20.0	50.0	1.0	380.5
C19	700	Humic ac.	1.0	50.0	1.0	460.2
C20	400	Humic ac.	1.0	10.0	1.0	–
C21	400	Humic ac.	20.0	10.0	1.0	–
C22	700	Humic ac.	1.0	10.0	3.0	278.8
C23	550	Humic ac.	10.5	30.0	2.0	349.0
C24	550	Humic ac.	6.5	30.0	2.0	360.0
C25	700	Humic ac.	1.0	50.0	3.0	512.9
CR1	700	Resin 1	20.0	25.0	3.0	–
CR2	700	Resin 2	20.0	25.0	3.0	–
CAR	700	Clay	20.0	25.0	3.0	–
CH	700	Humic ac.	20.0	25.0	3.0	–

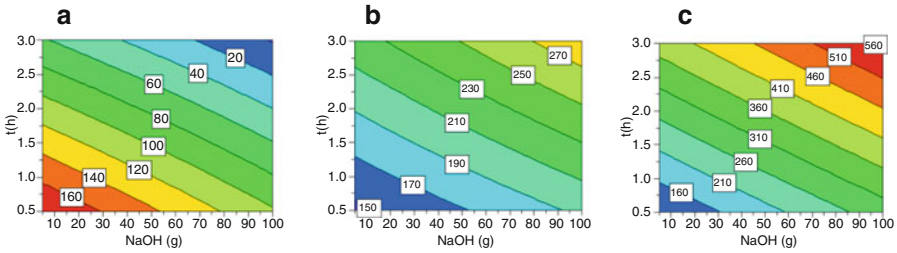

Fig. 6.1 Response surface values obtained using linear planning at pyrolysis temperatures of (**a**) 300 °C, (**b**) 500 °C, and (**c**) 700 °C (Gómez-Pacheco et al. 2012)

100 g), (B) pyrolysis temperature (from 300 °C to 700 °C), and (C) pyrolysis time (from 30 min to 3 h). The response considered was the capacity of the carbon to adsorb tetracycline (q_e). The adsorption capacity was obtained by using a tetracycline initial concentration of 700 mg/L, 0.1 g of adsorbent and 0.1 L of solution volume.

For the study of factor A (amount of NaOH added), experiments were conducted with fixed values of B (300 °C) and C (0.5 h) but two different values of A (5 and 100 g), allowing any variations in the response to be attributed to factor A (Samples C1′ and C2′ in Table 6.3). The same procedure was carried out for the other two factors. Figure 6.1 depicts the response surface obtained using linear planning to prepare the adsorbents from sludge. The maximum adsorption capacity of these adsorbents (in red) was obtained with pyrolysis for 3 h at a constant temperature of 700 °C, reaching a tetracycline adsorption capacity of 560 mg/g. As shown in Fig. 6.1a, a low adsorption capacity was found in samples pyrolyzed at a temperature of 300 °C, observing a decrease in adsorption capacity with longer pyrolysis time or higher NaOH concentration; the opposite behaviors to those observed at a pyrolysis temperature of 500 °C or 700 °C.

Optimization of Sludge Activation Process with Binder (Orthogonal Model)

Preparation of adsorbent materials by sludge chemical activation requires the addition of a binder to facilitate inter-particle union and obtain materials with suitable mechanical properties for application in water treatments. We investigated the effect of the binder on the adsorption capacity of these materials using orthogonal planning (MODDE 7.0 program) to study response surface values (Hunter and Hunter 1978). Figure 6.2 shows the response surface obtained to prepare these materials, maintaining a constant amount of NaOH (25 g) for different pyrolysis times (1, 2, and 3 h, respectively).

Figure 6.2 shows that the optimal values (in red) for the adsorption capacity of the activated carbon were 500 °C and 20 g of binder or 700 °C and 2 g of binder, achieving a tetracycline adsorption capacity of 470 mg/g. The results depicted in Fig. 6.2b show that the adsorption capacity of these materials increases with higher

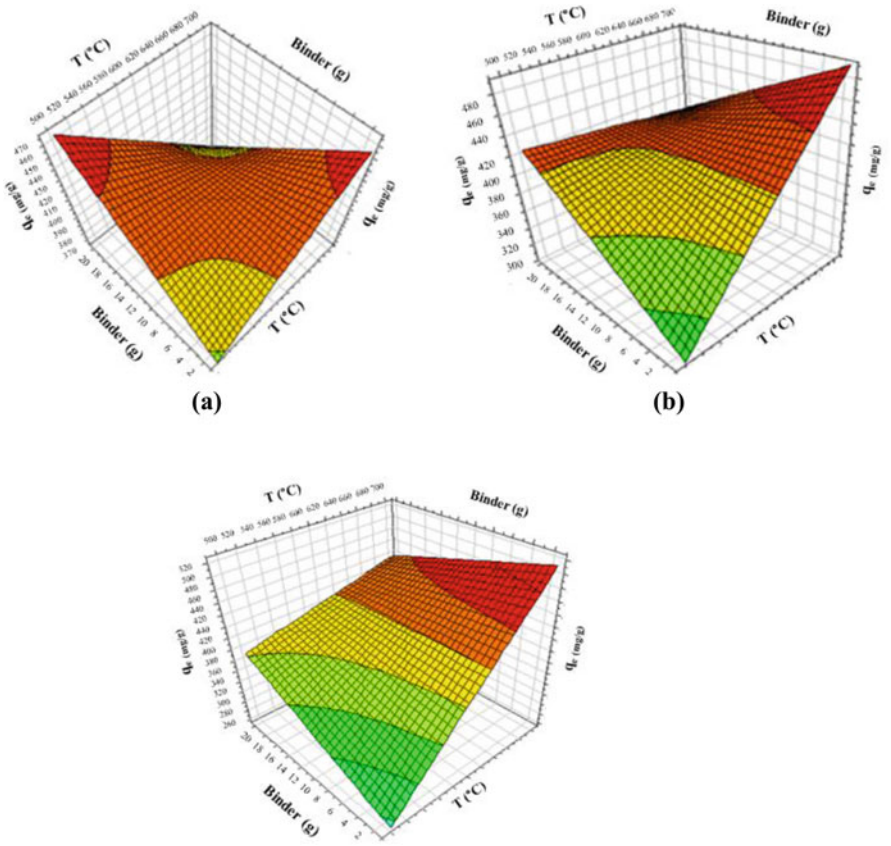

Fig. 6.2 Response surface by orthogonal planning, maintaining a constant amount of NaOH (25 g): (**a**) 1 h of pyrolysis, (**b**) 2 h of pyrolysis, (**c**) 3 h of pyrolysis. V = 100 mL, C_{A0} = 700 mg/L, m = 0.1 g (Gómez-Pacheco et al. 2012)

pyrolysis temperatures and lower amounts of binder, reaching values close to 500 mg/g. The absence of binder in the sample may increase the external surface area available for the adsorbate.

The results in Fig. 6.2c show that the optimal surface increases with higher pyrolysis temperature, and the model predicts that a good adsorption is even maintained with larger amounts of binder. These findings indicate that samples pyrolyzed at high temperatures for 3 h have good adsorbent properties, reaching values above 400 mg/g, even with a large amount of binder.

6.2.2.3 Characterization of Sludge-Derived Adsorbent Materials

Table 6.4 lists the results of the chemical analysis of the baseline sludge; it had a high content of organic matter (64.0%) and total nitrogen (7.8%) and metals, mainly zinc, copper, lead, and nickel. The textural and chemical properties of the sludge depend of the urban sludge considered. Sludge characterization is usually linked to the municipal and industrial activity of the city.

Textural Characterization of Adsorbents with Humic Acid as Binding Agent

Table 6.5 lists the values for surface area (S_{BET}) and mean micropore width (L_0) determined by N_2 adsorption at 77 K of the sludge-derived adsorbent materials containing humic acid as binder. The general behaviors shown in Table 6.5 are in agreement with previous reports (Méndez et al. 2005; Kang et al. 2006; Ros et al. 2006) on the use of chemical activation to prepare adsorbents from different raw materials:

Table 6.4 Chemical analysis of the dehydrated sludge (Gómez-Pacheco et al. 2012)

Component	% (by weight)	Component	μg/g
Dry matter	27.0	Cadmium	1.0
Organic matter	64.0	Chrome	2.7
pH	7.7	Copper	270.0
Total nitrogen	7.8	Lead	75.0
Phosphorus	3.8	Zinc	544.0
Calcium	0.3	Nickel	16.5
		Mercury	1.0

Table 6.5 Surface area and mean micropore width of the adsorbent materials prepared with humic acid as binder (Gómez-Pacheco et al. 2012)

Sample	Temperature (°C)	Activation time (h)	Binder (g)	NaOH (g)	S_{BET} (m^2/g)	$L_0(N_2)$ (nm)
C25	700	3	1.0	50	105	1.76
C3	700	3	10.0	25	175	2.25
C22	700	3	1.0	10	94	1.74
C9	700	3	20.0	50	124	1.90
C5	700	3	20.0	25	164	1.13
C12	700	3	20.0	10	104	1.28
C8	550	2	10.5	30	59	2.29
C23	550	2	10.5	30	61	2.20
C24	550	2	6.5	30	97	2.15
C16	700	1	20.0	50	87	1.75
C15	700	1	20.0	10	85	1.83
C19	700	1	1.0	50	87	1.79
C13	700	1	1.0	10	103	1.28

(i) The surface area of these materials was very low, with values ranging from 164 to 59 m^2/g, indicating the low effectiveness of the chemical activation of sludge in comparison to that of other adsorbent materials from sludge, with surface areas of 1000 m^2/g (Ros et al. 2006) or 380 m^2/g (Wang et al. 2008b).
(ii) Regardless of the sample in question, the surface area was enlarged with higher temperature or longer activation time.
(iii) Regardless of the amount of binder added, the surface area value was always higher for samples prepared with 25 g NaOH (sludge: NaOH ratio of 100:25 by weight).

Results in Table 6.5 show the optimal values for activating and binding agents to prepare adsorbent materials from sludge, considering the surface area value as response. As an example, Fig. 6.3 depicts the results obtained by applying the statistical optimization model at a pyrolysis temperature of 700 °C and a residence time of 3 h. As can be observed, the surface area of the materials increases with the amount of NaOH and, especially, with the amount of binder. The optimal experimental conditions are 3 h of pyrolysis at 700 °C with 30 g NaOH and 20 g of binder. As observed in Fig. 6.3, the surface area of these materials is not strongly influenced by the amount of NaOH and is most influenced by the amount of binder.

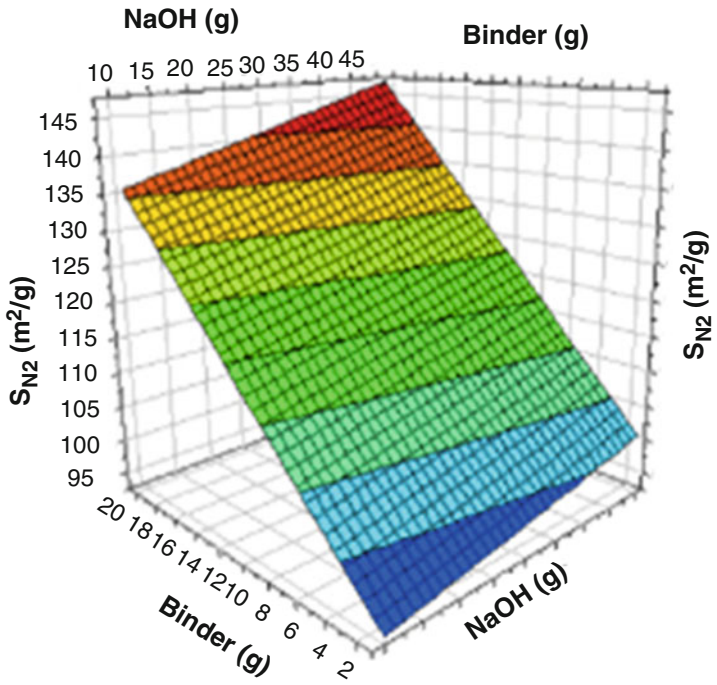

Fig. 6.3 Surface obtained with pyrolysis at 700 °C for 3 h, applying the statistical model to optimize adsorbent material preparation (Gómez-Pacheco et al. 2012)

Table 6.6 Textural characteristics of sludge-derived adsorbents with humic acid as binder (Gómez-Pacheco et al. 2012)

Sample	$W_0(N_2)$ (cm^3/g)	$W_0(CO_2)$ (cm^3/g)	$L_0(N_2)$ (nm)	$L_0(CO_2)$ (nm)	$W_0(N_2)/W_0(CO_2)$
C2	0.06	0.05	1.97	0.50	1.20
C3	0.06	0.02	2.25	1.25	3.00
C5	0.06	0.05	1.13	0.47	1.20
C8	0.03	0.04	2.29	0.50	0.75
C9	0.05	0.06	1.90	0.48	0.83
C12	0.04	0.06	1.28	0.50	0.67
C13	0.04	0.05	1.24	0.49	0.80
C15	0.04	0.06	1.83	0.52	0.67
C16	0.03	0.04	1.75	0.48	0.75
C19	0.04	0.03	1.79	0.49	1.33
C22	0.04	0.05	1.74	0.49	0.80
C23	0.03	0.04	2.20	0.48	0.75
C24	0.03	0.04	2.15	0.49	0.75
C25	0.05	0.03	1.76	0.52	1.66

Table 6.6 lists the results of the textural analysis from N_2 and CO_2 adsorption isotherms, showing that the mean micropore width determined with CO_2 (all ~0.5 nm except for sample C3) is lower than that determined with N_2 (> 1.13 mm for all samples). This is due to the fact that CO_2 is only adsorbed in smaller size micropores (ultramicropores), whereas N_2 is adsorbed on the surface of greater size micropores (Garrido et al. 1987; Rodriguez-Reinoso and Linares-Solano 1989). In the majority of samples, the CO_2-determined micropore volume was larger than the N_2-determined micropore volume, indicating a very narrow microporosity that is not totally accessible to N_2 molecules under these experimental adsorption conditions.

Influence of Binding Agent on Properties of the Adsorbent Materials

After optimizing the preparation of these materials from sludge for their tetracycline adsorption capacity and surface area (response variables), we studied the influence of binder type on their properties. Samples were prepared using humic acid (CH), clayey soil (CAR), or phenolic resins (CR1 or CR2) as binder. Table 6.7 shows the textural characteristics of these samples and of a sample prepared without NaOH or binder (CL) and one prepared without binder (C2).

The results in Table 6.7 show that the surface area was increased by the activation, as discussed above. They reveal that the textural properties of these materials were not substantially affected by the addition of phenolic resins as binding agents, with samples C2 (reference), CH, CR1 and CR2 having similar textural features. However, we highlight the similar surface areas of sample CAR

Table 6.7 Textural characteristics of adsorbent materials prepared with different binders (Gómez-Pacheco et al. 2012)

Samples	S_{BET} (m^2/g)	$W_0(N_2)$ (cm^3/g)	$W_0(CO_2)$ (cm^3/g)	$L_0(N_2)$ (nm)	$L_0(CO_2)$ (nm)	$W_0(N_2)/W_0(CO_2)$
CL	47	0.02	0.03	1.18	0.99	0.67
C2	139	0.06	0.05	1.97	0.50	1.20
CH	163	0.06	0.05	1.13	0.47	1.20
CAR	62	0.03	0.02	1.24	1.35	1.50
CR1	147	0.06	0.03	1.13	0.83	2.00
CR2	152	0.07	0.03	1.16	0.95	2.33

Table 6.8 Adsorbent characteristics obtained by mercury porosimetry (Gómez-Pacheco et al. 2012)

Sample	S_{ext} (m^2/g)	V_2[a] (cm^3/g)	V_3[b] (cm^3/g)	ρ_a[c] (g/cm^3)
CL	31.39	0.07	0.19	0.16
C2	134.02	0.29	1.54	0.09
CH	44.65	0.12	0.24	0.18
CAR	106.77	0.20	0.78	0.13
CR1	163.21	0.38	0.45	0.10
CR2	102.98	0.27	0.66	0.10

[a]V_2 Volume of pores with diameter of 6.6–50 nm determined by mercury porosimetry
[b]V_3 Volume of pores with diameter >50 nm determined by mercury porosimetry
[c]ρ_a Apparent density determined by mercury porosimetry

and the sample CL, which was not NaOH-activated, indicating that the surface area was reduced by the presence of clayey soil in the sample. In general, samples had a larger micropore volume by N_2 than by CO_2 determination, reflecting a heterogeneous distribution of microporosity in these materials.

Table 6.8 exhibits the pore volumes of the adsorbent materials obtained by mercury porosimetry. Except for the development of mesoporosity in sample CR1, the mesoporosity (V_2) and macroporosity (V_3) of all samples decreased with the presence of the binder, especially with humic acid (sample CH). Table 6.9 shows the elemental analysis of the samples; all had a low C content that was higher with the presence of binders; it was only 5.76% in the sample without binder and around 18% in the samples with binder, with the exception of CAR. X-ray fluorescence results in Table 6.10 show SiO_2 and CaO to be the predominant inorganic compounds in these samples. The following components were identified in the X-ray diffraction diagrams: calcium pyrophosphate, β–$Ca_2P_2O_7$(peak at 30.8°2θ); calcium hydroxyapatite, $Ca_5(PO_4)_3OH$ (peak at 31.6° 2θ); goethite, α-FeOOH (peak at 21°2θ); and hematites, α-Fe_2O_3 (peak at 33° 2θ). The remaining oxides in Table 6.10 were not observed in the diagrams, possibly due to their lack of crystallinity. Table 6.9 compiles some chemical characteristics of the adsorbent material samples, which were predominantly of basic nature, with pH_{PZC} values ranging from 8.7 (CAR) to 10.3 (C2).

Table 6.9 Elemental analysis of the samples (dry basis) (Gómez-Pacheco et al. 2012)

Sample	C (%)	H (%)	N (%)	(O + remaining elements)$_{dif}$ (%)	pH_{PZC}
CL	23.09	1.05	1.87	73.99	9.6
C2	5.76	0.70	0.41	93.13	10.3
CH	18.25	1.06	1.29	79.40	9.4
CAR	5.13	1.05	0.00	93.82	8.7
CR1	17.75	1.11	0.62	80.52	8.9
CR2	17.80	1.11	1.06	80.03	8.9

6.2.3 Activated Carbons from Petroleum Coke

Petroleum coke is a dark solid composed mainly of carbon, produced by the thermal decomposition and polymerization of heavy liquid hydrocarbon derived from crude oil. The coke produced from distillation residues tends to form the sponge coke, while coke produced from a cracking residue forms the premium coke. The sponge type, due to its practically amorphous structure, has little commercial value and may be an economical and environmental problem. Petroleum coke is a residue of the petrochemical industry, which generates around 4 tons of carbon for every 100 tons of crude oil refined. Because of its high concentration of heavy metals (Ni, V, Fe), this residue cannot be used in any productive process. However, due to its high carbon content, it is an excellent raw material for the production of activated carbon.

6.2.3.1 Preparation of Activated Carbons by Chemical Activation of Coke

A series of activated carbons were prepared from calcinated petroleum coke supplied by REPSOL-YPF (Alicante, Spain). This coke will be designated as C, and its particle size ranged from 0.5 to 0.8 mm.

KOH was used as activating agent for the petroleum coke activation. Different activated cokes were prepared, with a KOH/coke mass ratio ranging from 1 to 4. The samples will be designated with the letter C followed by the KOH/coke mass ratio used in the activation process.

The procedure described by Otowa et al. (1993) was used for the coke activation. Briefly, 25 g of petroleum coke was mixed with 100 mL of a KOH solution at the appropriate concentration for each sample. This mixture was first heated at 60 °C for 48 h and was then treated in N_2 atmosphere (flow 300 mL/min) at 400 °C for 2 h. Finally, it was carbonized by heating the mixture at 700 °C for 1 h under an N_2 flow of 300 mL/min. In all heat treatments, the oven heating rate was 10 °C/min. Finally, the samples were washed with deionized water to constant conductivity.

Table 6.10 Adsorbent characteristics obtained by X-ray fluorescence (Gómez-Pacheco et al. 2012)

Sample	SiO_2 (%)	Al_2O_3 (%)	Fe_2O_3 (%)	MnO (%)	MgO (%)	CaO (%)	Na_2O (%)	K_2O (%)	TiO_2 (%)	P_2O_5 (%)	LOI (%)
C2	23.75	11.65	9.64	0.06	4.13	21.81	3.42	0.15	1.00	11.29	12.41
CH	21.24	10.47	11.22	0.06	3.54	18.10	5.96	0.11	0.94	9.78	17.68
CAR	27.15	13.39	11.00	0.10	5.35	11.46	4.37	0.25	1.03	11.53	13.61
CR2	23.44	9.55	11.26	0.08	4.53	16.59	2.00	0.16	0.97	8.24	22.74

LOI loss on ignition

6.2.3.2 Characterization of Activated Carbons from Coke

Elemental analysis of the petroleum coke used was done with a Fisons Instruments 1108 CHNS analyzer and showed a composition of C = 87.7 ± 0.1%, H = 4.2 ± 0.1%, N = 0.4 ± 0.1%, S = 6.4 ± 0.1%, and O = 1.3 ± 0.1%.

Table 6.11 shows the results of the textural characterization of the activated carbons prepared with different KOH/coke mass ratios and of both original and demineralized cokes. These results indicate that the activation process considerably developed the porosity in all of the samples studied, increasing the volume of micro-, meso- (V_2), and macropores (V_3). Thus, the surface area of the original coke markedly increased after the activation, with sample C-1 showing the highest value. Moreover, it was observed that the micropore volume reduced with an increase in the amount of KOH added to the coke; the K_2O and K generated during the activation blocked the entrance to the pores, hampering the diffusion of CO_2 into a fraction of the micropores, as discussed below.

The value of S_{BET} was always higher than the value of micropore surface area (S_{mic}) regardless of the activated coke sample considered (Table 6.11). According to these results, a large fraction of the surface of these four samples corresponded to meso- and macropores, which are determined by N_2 at 196 °C but not by CO_2 at 0 °C (Garrido et al. 1987; Rodriguez-Reinoso and Linares-Solano 1989). Thus, the proportion of this fraction ranged from 41% in sample C-4 to 5% in sample C-1. It was also observed that the volume of macropores (V_3) was slightly larger when the amount of KOH in the samples was increased, whereas the volume of micro- and mesopores reduced with increases in the amount of KOH.

Several authors have studied the mechanism by which KOH activates carbonaceous materials (Marsh et al. 1984; Otowa et al. 1997). Thus, Marsh et al. (1984) showed that the oxygen of the alkali can remove cross-linking and stabilizing carbon atoms in crystallites. K metal obtained at the reaction temperatures may intercalate and force apart the separate lamellae of the crystallites. The microporosity of activated carbon in the new structure is created by the removal of potassium salts by washing and the removal of carbon atoms from the internal volume of the carbon by activation reaction. The results presented in Table 6.11 indicate that W_0 and S_{BET} values decreased with an increase in the KOH/coke

Table 6.11 Textural characterization of the original and activated cokes (Sánchez-Polo and Rivera-Utrilla 2006)

Sample	KOH/coke	S_{BET} (m^2/g)	S_{mic}[a] (m^2/g)	$W_0(N_2)$ (cm^3/g)	V_2 (cm^3/g)	V_3 (cm^3/g)
C	0	<30	<30	0.02 ± 0.01	Nil	0.011 ± 0.003
C-1	1	1619 ± 30	1539 ± 30	0.55 ± 0.01	0.063 ± 0.003	0.132 ± 0.003
C-2	2	1261 ± 30	1165 ± 30	0.41 ± 0.01	0.061 ± 0.003	0.154 ± 0.003
C-3	3	1021 ± 30	716 ± 30	0.25 ± 0.01	0.058 ± 0.003	0.176 ± 0.003
C-4	4	970 ± 30	569 ± 30	0.20 ± 0.01	0.051 ± 0.003	0.263 ± 0.003

[a]Micropore surface area obtained from CO_2 adsorption isotherm at 273.15 K

ratios, which may be due to a blockage of the pores by remains of the K and K_2O that were generated during the activation process and not completely removed by the washing treatment. As reported above, the macroporosity of the coke increases with a higher KOH/coke ratio in the activation process. According to Otowa et al. (1993), elevated temperatures and high KOH/coke ratios produce large pores in the carbon structure due to the presence of KOH-derived K_2O, which expands the carbon atomic layers. K_2O also acts as catalyst of the carbon gasification process, so that its generation during petroleum coke activation potentiates the development of meso- and macroporosity on the carbon surface. Moreover, at temperatures above 700 °C, a considerable amount of K is formed by the reduction of K_2O with carbon (Otowa et al. 1993). As a result of the consumption of the inner carbon atoms, pores are formed in the structure.

Regarding the surface chemistry of the samples, it was observed that activation of the coke modified their chemical nature (Table 6.12). Thus, whereas the original coke was a mildly acid material ($pH_{PZC} = 6.5$), the pH_{PZC} of the KOH-activated coke ranged from 8.4 for sample C-1 to 9.7 for sample C-4. This change is largely due to the generation of surface basic groups during the activation process which increases with the KOH/coke ratio (Table 6.12). Nevertheless, the pH_{PZC} values, as with the above textural characteristics, might be slightly influenced by the presence of K and K_2O in the activated coke samples. In order to know it, the ash content of the activated coke samples was determined. The results obtained, 0.40%, 0.42%, 0.46%, and 0.52% for the samples C-1, C-2, C-3, and C-4, respectively, indicated a slight increase in the ash content as the KOH/coke ratio was increased. Therefore, as mentioned above, the presence of these species of K can influence, in part, on the basicity of the activated coke samples.

The functional groups generated on the carbon surface during activation were studied by means of X-ray photoemission spectroscopy (Table 6.13). The results

Table 6.12 pH_{PZC} of the activated cokes (Sánchez-Polo and Rivera-Utrilla 2006)

Sample	pH_{PZC}
C	6.5 ± 0.1
C-1	8.4 ± 0.1
C-2	8.8 ± 0.1
C-3	9.3 ± 0.1
C-4	9.7 ± 0.1

Table 6.13 Results of the deconvolution of the XPS O1s spectrum of the activated coke samples (Sánchez-Polo and Rivera-Utrilla 2006)

Sample	(- C = O) (%) 530.7 ± 0.2 eV	(C - OH, C – O - C) (%) 532.1 ± 0.2 eV	(- COOH) (%) 533.3 ± 0.2 eV	H_2O and/or O_2 (%) 535.3 ± 0.2 eV
C-1	76 ± 1	14 ± 1	6 ± 1	4 ± 1
C-2	80 ± 1	8 ± 1	8 ± 1	4 ± 1
C-3	84 ± 1	8 ± 1	3 ± 1	5 ± 1
C-4	90 ± 1	4 ± 1	2 ± 1	4 ± 1

showed a percentage of surface oxygen of around 10% in all the activated coke samples, much higher value than the percentage detected by elemental analysis in the original coke (% O = 1.3), which would confirm the creation of oxygen groups on the coke during its KOH activation.

In order to determine the surface functional groups generated by the activation process, the spectrum of the O1s region was studied in the activated coke samples following the method described elsewhere (Moreno-Castilla et al. 2003b). The results obtained are shown in Table 6.13. In the four samples, the oxygen percentage corresponding to the –COOH group, which is the main responsible group of the surface acidity, is very low. This fact may be due to the low thermal stability of this group (242–367 °C), which may be desorbed in the form of CO, CO_2, and H_2O during the activation process (Zielke et al. 1996); these results justify the pH_{PZC} values found for the activated coke samples. As the KOH/coke ratio increased, the concentration of –C = O on the activated coke sample also increased. These results explain, in part, the enhancement in the surface basicity as the KOH/coke used in the activation process increased.

6.3 Kinetic Study of the Adsorption of Tetracyclines and Nitroimidazoles on Sludge-Derived Materials and Activated Carbons

6.3.1 Tetracyclines and Nitroimidazoles Characterization

6.3.1.1 Tetracyclines

The tetracyclines (TCs) studied in this chapter were tetracycline (TC), oxytetracycline (OTC), and chlortetracycline (CTC). The chemical structures of the TCs are depicted in Fig. 6.4a, and their physicochemical properties are summarized in Table 6.14. Additionally, the speciation diagram of TC as a function of solution pH is shown in Fig. 6.4b, as an example.

6.3.1.2 Nitroimidazoles

Nitroimidazoles used in the present study were dimetridazole (DMZ), metronidazole (MNZ), ronidazole (RNZ), and tinidazole (TNZ). Figure 6.5 depicts the molecular structure and speciation diagrams of these compounds. Dimensions of the nitroimidazole molecules were determined with the computer software Advanced Chemistry Development (ACD/Labs) Software v8.14. Octanol-water partition coefficients (K_{OW}) were obtained from ChemIDplus Advanced database. Table 6.15 lists the main physicochemical properties of nitroimidazoles.

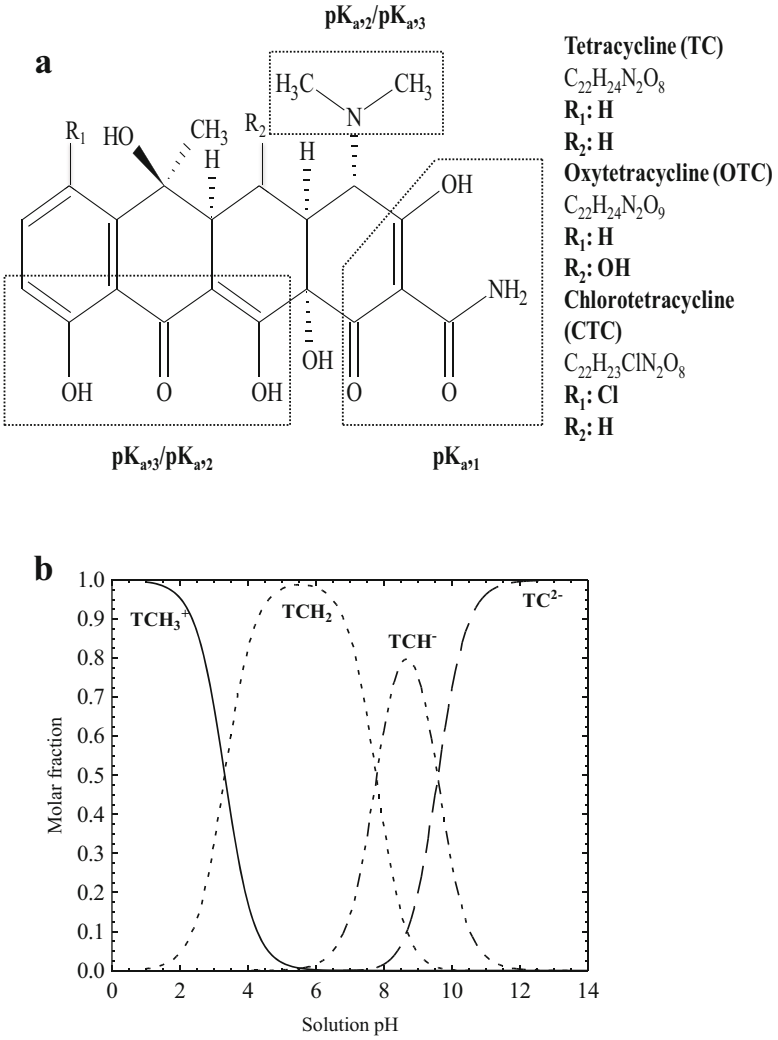

Fig. 6.4 Molecular structure (**a**) and speciation diagram (**b**) of tetracyclines in aqueous solution

6.3.2 Kinetic and Diffusional Models

In kinetic models, it is usually assumed that the overall adsorption rate is exclusively controlled by the adsorption rate of the solute on the adsorbent surface, and the intraparticle diffusion and external mass transport can be ignored. It is also considered that the adsorption rate of a solute on the surface can be represented in the same manner as the rate of a chemical reaction. As stated in Chap. 3, adsorption kinetics are commonly interpreted with first- and second-order kinetic models. On the other hand, diffusional models assume the adsorption process to occur by means

Table 6.14 Physicochemical properties of TCs

TCs	Molecular volume[a] (A^3)	Cross-sectional area[a] (A^2)	Water solubility[b] (mg/L)	Log K_{ow}[b]	pK_a[b]
TC	403.72	396.90	22	−1.30	3.32 7.78 9.58
OTC	413.13	407.49	17	−0.90	3.22 7.46 8.94
CTC	416.90	410.50	4.2	−0.62	3.33 7.55 9.33

[a]Determined by applying a Monte Carlo algorithm with the Spartan08 program
[b]Determined by means of the Advanced Chemistry Development (ACD/Labs) Software v8.14 program. pK_a corresponding to the successive deprotonation reactions

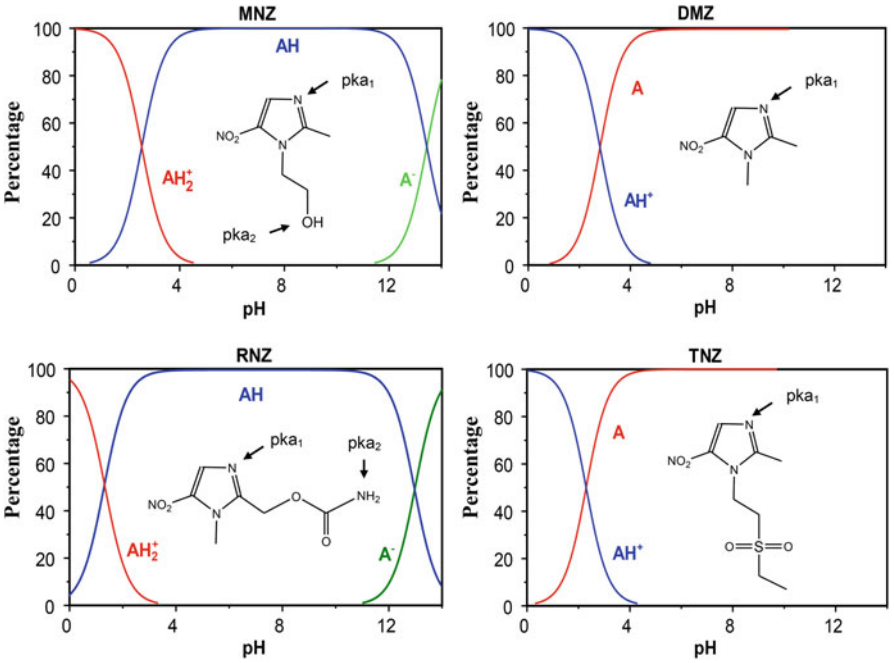

Fig. 6.5 Chemical structure and speciation diagram of nitroimidazoles

of three well-differentiated steps: (i) external mass transfer, where the adsorbate is transferred from the bulk of the solution to the adsorbent external surface; (ii) intraparticle diffusion, where the adsorbate molecule diffuses through the pores from the external surface of the adsorbent particle to the adsorption sites; and iii) adsorption rate of the compound on an active site (Leyva-Ramos and Geankoplis 1985). In this last step, the adsorption equilibrium between solute in

Table 6.15 Properties of nitroimidazoles

Nitroimidazole	Molecular weight (g/mol)	Transversal section (A^2)	$D_{AB} \times 10^6$ (cm^2/s)	Volume (A^3)	Solubility in water (mol/L)	pK_{ow}	pK_{a1}	pK_{a2}
MNZ	171.15	101	9.63	186	0.041	0.02	2.58	14.44
DMZ	141.13	88	8.48	157	0.062	−0.31	2.81	–
TNZ	247.27	138	8.25	258	0.008	0.35	2.30	–
RNZ	200.15	113	6.72	206	0.015	0.38	1.32	12.99

solution and solute on adsorbent is considered to be instantaneous (Ocampo-Perez et al. 2010); therefore the amount of solute adsorbed on the pore surface is at equilibrium with the solute concentration in the solution. Under these conditions, external transfer and/or intraparticle diffusion will be largely responsible for the global adsorption rate. In the following sections, the most important kinetic models and diffusional models used to predict the concentration decay curves for several adsorbate-adsorbent systems will be discussed in detail. Note that details of adsorption kinetic models have been also covered in Chap. 3 of this book.

6.3.2.1 Pseudo First-Order Kinetic Model

Lagergren advanced the first-order kinetic model to predict the adsorption rate of oxalic and malonic acids onto charcoal (Ho and Mckay 1998). The pseudo first-order kinetic model has been extensively applied to interpret the adsorption rate of solutes on different adsorbents (Srivastava et al. 2006). The pseudo first-order kinetic model can be mathematically represented by the following equation:

$$\frac{dq_t}{dt} = k_1(q_e - q_t) \tag{6.1}$$

where k_1 is the rate constant of the pseudo first-order kinetic model (1/h), t is the time (min), and q_e and q_t are the mass of adsorbate adsorbed at the equilibrium and at time t (mg/g), respectively.

This equation can be integrated using the initial condition $q_t = 0$ when $t = 0$, and the resulting equation is:

$$q_t = q_e\left(1 - e^{-k_1 t}\right) \tag{6.2}$$

The above equation can also be expressed in terms of C_A and C_{Ae} by using the mass balance equation at time t and equilibrium as follows:

$$q_t = \frac{V(C_{A0} - C_A)}{m} \tag{6.3}$$

$$q_e = \frac{V(C_{A0} - C_{Ae})}{m} \tag{6.4}$$

where V is the volume of the solution (L); C_{A0}, C_A, and C_{Ae} are the initial, at a time t and the equilibrium concentration of adsorbate in aqueous solution (mg/L); and m is the mass of adsorbent (g). These mathematical relationships can be substituted into Eq. (6.2), and the following equation can be obtained:

$$C_A = C_{A0} - \left(\frac{m}{V}\right) q_e \left(1 - e^{-k_1 t}\right) \tag{6.5}$$

6.3.2.2 Pseudo Second-Order Kinetic Model

The pseudo-second-order kinetic model can be represented by the following differential equation (Blanchard et al. 1984):

$$\frac{dq_t}{dt} = k_2 (q_e - q_t)^2 \tag{6.6}$$

where k_2 is the rate constant of the pseudo-second-order kinetic model (g/mg/h).

Integrating Eq. (6.6) and using the initial condition $q_t = 0$ when $t = 0$, the following equation can be obtained:

$$q = \frac{q_e^2 k_2 t}{1 + q_e k_2 t} \tag{6.7}$$

This equation can be also formulated in terms of C_A and C_{A0}, yielding the following equation:

$$C_A = C_{A0} - \left(\frac{m}{V}\right) \frac{q_e^2 k_2 t}{1 + q_e k_2 t} \tag{6.8}$$

6.3.2.3 Intraparticle Diffusion Model

A functional relationship common to most treatments of intraparticle diffusion is that uptake varies almost proportionately with the half-power of time ($t^{0.5}$), rather than t. Good linearization of the data is observed for the initial phase of the reaction in accordance with expected behavior if intraparticle diffusion is the rate-limiting step (Ho and Mckay 1998; Ip et al. 2010). The intraparticle diffusion equation is the following:

$$q_t = k_i t^{0.5} \tag{6.9}$$

where k_i is the intraparticle diffusion rate constant ($mg/g^{-1}h^{-0.5}$).

The k_i values are calculated from the slope of the straight line of the respective plots. The plot of q_t versus $t^{0.5}$ may present multi-linearity, which indicates that two or more rate controlling steps occur in the adsorption process.

6.3.2.4 Surface and Pore Volume Diffusion Model

The diffusional model is based on the following assumptions: (i) the intraparticle diffusion occurs by pore volume diffusion (Fick diffusion) and surface diffusion, (ii) the rate of adsorption on an active site is instantaneous, and (iii) the adsorbent particles are spherical. The model equations and initial and boundary conditions are the following (Leyva-Ramos and Geankoplis 1994; Ocampo-Perez et al. 2011):

$$V\frac{dC_A}{dt} = -mSk_L\left(C_A - C_{Ar}|_{r=R_p}\right) \tag{6.10}$$

$$t = 0 \qquad C_A = C_{A0} \tag{6.11}$$

$$\varepsilon_p\frac{\partial C_{Ar}}{\partial t} + \rho_p\frac{\partial q}{\partial t} = \frac{1}{r^2}\frac{\partial}{\partial r}\left[r^2\left(D_{ep}\frac{\partial C_{Ar}}{\partial r} + D_s\rho_p\frac{\partial q}{\partial r}\right)\right] \tag{6.12}$$

$$C_{Ar} = 0 \qquad t = 0 \qquad 0 \le r \le R_p \tag{6.13}$$

$$\left.\frac{\partial C_{Ar}}{\partial r}\right|_{r=0} = 0 \tag{6.14}$$

$$D_{ep}\left.\frac{\partial C_{Ar}}{\partial r}\right|_{r=R} + D_s\rho_p\frac{\partial q}{\partial r} = k_L\left(C_A - C_{Ar}|_{r=R_p}\right) \tag{6.15}$$

where S is the external surface area determined from $S = 3/(R_p \times \rho_p)$, R_p is the radius of the particle (cm), k_L is the external mass transfer coefficient in liquid phase (cm/s), R is the distance in radial direction of the particle (cm), $C_{Ar}\,/_{r=R}$ is the concentration of adsorbate at the external surface of the particle at $r = R$ (mg/L), ε_p is void fraction of particles, C_{Ar} is the concentration of adsorbate within the particle at distance r (mg/L), ρ_p the density of adsorbent particles (g/mL), D_{ep} is the effective pore volume diffusion coefficient (cm^2/s), D_s is the surface diffusion coefficient (cm^2/s), and q is the adsorption capacity (mg/g).

The Eqs. (6.10), (6.11), (6.12), (6.13), (6.14), and (6.15) represent the pore volume and surface diffusional model (PVSDM). The parameters k_L, D_S, and D_{ep} correspond to external mass transport, surface diffusion, and pore volume diffusion mechanisms, respectively. The PVSDM model can be simplified by considering that the intraparticle diffusion mechanism may be exclusively due to either pore volume diffusion (PVDM) ($D_{ep} \neq 0, D_S = 0$) or surface diffusion (SDM) ($D_{ep} = 0$, $D_S \neq 0$).

If the adsorption rate on an active site is considered to be instantaneous, there is local equilibrium between the adsorbate concentration in the solution within the pore of the adsorbent and the mass of adsorbate adsorbed on the surface of the pore. This equilibrium relationship between C_{Ar} and q_m is represented by the adsorption isotherm:

$$q_m = f(C_{Ar}) \tag{6.16}$$

6.3.3 *Results and Discussion*

6.3.3.1 Kinetic Study of Tetracycline Adsorption on Sludge-Derived Adsorbents

Adsorption kinetics were obtained by adding 0.1 g adsorbent material in Erlenmeyer flasks that contained 100 mL of a 700 mg/L TC solution. The flasks were maintained in thermostatic bath at 298 K and under agitation for 10 days, and samples were periodically extracted to determine the amount of TC adsorbed as a function of time. Solution pH ranged between 7 and 8 in all cases. Figure 6.6 depicts the adsorption kinetics of TC on selected sludge-derived adsorbents.

In order to quantify the rate of TC adsorption on the adsorbents and to identify the chemical and textural properties involved in this process, adsorption rate constants (k_1, k_2) were determined by fitting the experimental adsorption kinetics data to pseudo first-order and second-order kinetic models, respectively. Table 6.16 shows the results obtained and also the values of the amounts of TC adsorbed at equilibrium and the corresponding determination coefficients. A comparison between q_e values (theoretically calculated) and the corresponding q_e values (experimental) shows that the pseudo-first-order model fits the experimental data for all TC-adsorbents systems better than does the pseudo-second-order model.

The adsorption rate constants (k_1) (Table 6.16) were related to some of the characteristics of the corresponding adsorbents (Tables 6.7, 6.8, and 6.9). In general, no clear relationship was observed between the k_1 values and most of the textural parameters of the adsorbents, except for a tendency to higher k_1 values with increased pore volume, V_2, and macropore volume, V_3 (see Fig. 6.7a, b, respectively).

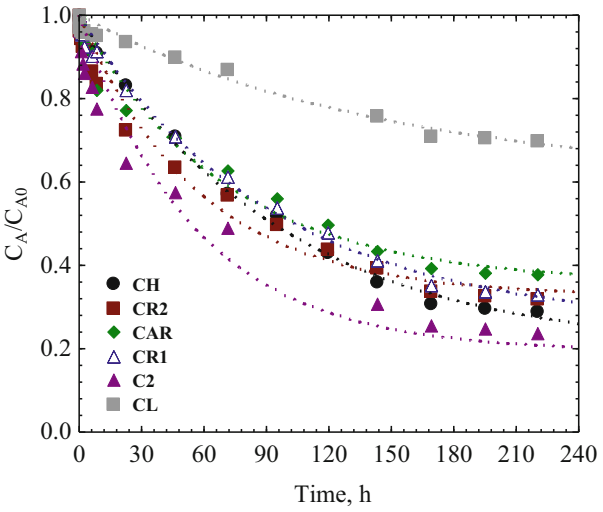

Fig. 6.6 TC adsorption kinetics on the adsorbents. pH ≈ 7, $[TC]_o = 700$ mg/L, T = 298 K. The *lines* represent the predictions of the first-order kinetic model (Ocampo-Pérez et al. 2012)

Table 6.16 Adsorption rate constants, determination coefficients, and amounts of TC adsorbed at equilibrium obtained experimentally and according to pseudo-first-order, pseudo-second-order, and intraparticle diffusion models (Ocampo-Pérez et al. 2012)

	Pseudo-first order				Pseudo-second order			Intraparticle diffusion	
Adsorbent	q_e (exp.) (mg/g)	$k_1 \times 10^2$ (1/h)	R^2	q_e (predicted) (mg/g)	$k_2 \times 10^5$ (L (mg/h)	R^2	q_e (predicted) (mg/g)	k_i (mg/(g $h^{0.5}$))	R^2
CL	210	0.68 ± 0.24	0.978	278 ± 55	1.11 ± 0.79	0.978	424 ± 110	10.82	0.952
C2	532	2.60 ± 0.079	0.955	565 ± 43	12.1 ± 3.8	0.977	537 ± 31	45.33	0.992
CH	497	1.04 ± 0.095	0.997	565 ± 23	2.16 ± 0.51	0.993	638 ± 42	31.12	0.977
CAR	434	1.42 ± 0.022	0.988	450 ± 26	2.81 ± 0.76	0.991	555 ± 40	31.50	0.982
CR1	469	1.08 ± 0.012	0.995	521 ± 27	3.89 ± 1.25	0.986	518 ± 40	29.93	0.980
CR2	476	1.73 ± 0.026	0.988	472 ± 23	4.37 ± 1.03	0.992	543 ± 29	37.50	0.991

TC adsorption rate constants also increased with lower carboxylic group content of the adsorbents (Fig. 6.7c), but no relationship was observed with the other chemical parameters of the adsorbents, such as the pH_{PZC} or basic group content. According to these findings, carboxylic groups in these materials reduce the adsorption rate because, at the working pH of 7–8, repulsive interactions are established between the negative charge of these groups and TC molecules, which are negatively charged as a consequence of deprotonation (see Fig. 6.4b).

The mechanism of adsorption is generally considered to involve (i) mass transfer of adsorbate from the bulk phase to particle surface, (ii) adsorption on surface site, and (iii) intraparticle diffusion of the adsorbate molecules to an adsorption site by a pore diffusion and/or surface diffusion mechanism. Step (ii) is often assumed to be extremely rapid; therefore the adsorption of large molecules, with long contact times to equilibrium, is always considered to be via diffusion controlled by external film resistance and/or internal diffusion mass transport or intraparticle diffusion.

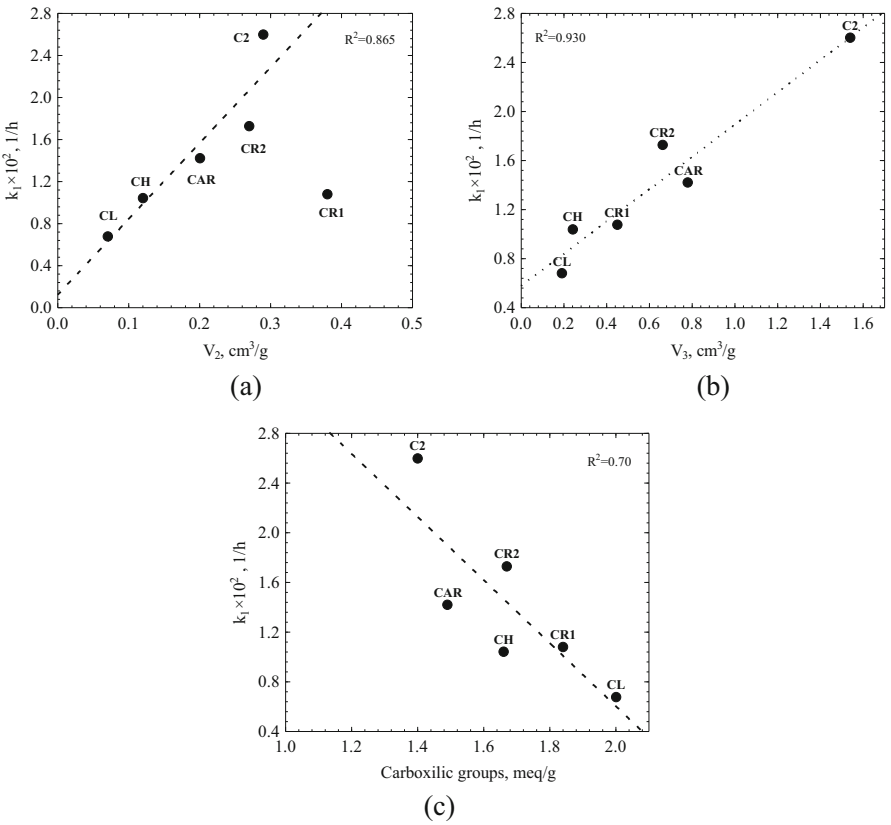

Fig. 6.7 Variation of k_1 with textural and chemical parameters of adsorbents (Ocampo-Pérez et al. 2012)

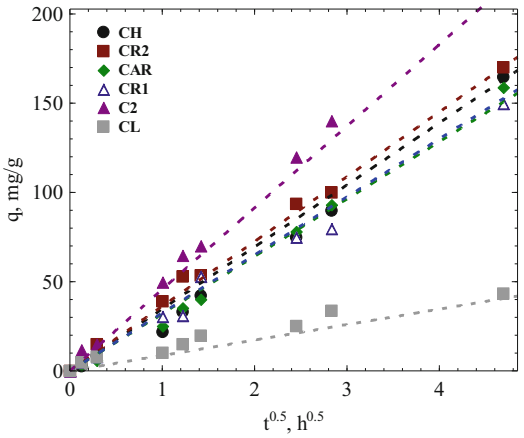

Fig. 6.8 Root time plot for the adsorption of tetracycline on the adsorbents. pH ≈ 7, $[TC]_o = 700$ mg/L, T = 298 K (Ocampo-Pérez et al. 2012)

A classical approach to analyze whether an adsorption process is controlled by intraparticle diffusion is to plot the amount adsorbed versus the square root of time, $t^{0.5}$ for a short contact time, i.e., $q/q_e < 0.3$. If the plot is linear and passes through the origin, it indicates that intraparticle diffusion is controlling the rate of adsorption. Thus, Fig. 6.8 shows the amount of tetracycline adsorbed as a function of $t^{0.5}$ for the sludge-derived adsorbents. It can be seen that intraparticle diffusion model satisfactorily fitted the experimental data, obtaining a linear section that passes through the origin in a short time, indicating that tetracycline adsorption on these adsorbents is governed by intraparticle diffusion. The values of the intraparticle diffusion rate constant (k_i) are given in Table 6.16 together with determination coefficient values (R^2). The k_i values ranged from 10.82 mg/(g $h^{0.5}$) for sample CL to 45.33 mg/(g $h^{0.5}$) for sample C2.

Surface diffusion, i.e., the movement of the adsorbate through the solid surface, is influenced by the distribution of the solid and fluid phases, and the surface concentration gradients are the main driving force. The surface diffusion model (SDM) is the most widely used to interpret concentration decay curves of aromatic compounds on adsorbents (Traegner and Suidan 1989; Ganguly and Goswami 1996); it assumes that the intraparticle diffusion is exclusively due to surface diffusion and that there is no pore volume diffusion. For its part, pore volume diffusion refers to the movement of the adsorbate due to concentration gradients in the fluid phase (i.e., molecular mechanisms) and is affected by the geometry of pore. Hence, the pore volume diffusion model (PVDM) ignores surface diffusion and assumes that pore volume diffusion is the sole mechanism of intraparticle diffusion (Traegner and Suidan 1989).

The TC concentration decay curves were predicted with SDM and PVDM models. Values of the external mass transfer coefficient (k_L) and the effective diffusion coefficients (D_s and D_{ep}) were required to resolve both models. Experimental k_L values were estimated from Eq. (6.17), while D_s and D_{ep} were obtained by matching the numerical solution of the models to the experimental data. The

optimal values of D_s and D_{ep} were the values that best fitted the experimental data by minimizing the objective function given by Eq. (6.18).

$$\left[\frac{d\left(\frac{C_A}{C_{A0}}\right)}{dt}\right]_{t=0} = \frac{-mSk_L}{V} \tag{6.17}$$

$$\sum_{1}^{N}\left(\phi_{\text{exp}} - \phi_{\text{pred}}\right)^2 = \text{Minimum} \tag{6.18}$$

where ϕ_{exp} and ϕ_{pred} are the experimental dimensionless concentration of adsorbate in the solution and predicted with the diffusion models, respectively, and N is number of experimental data.

Figure 6.9 depicts the TC concentration decay curves on all adsorbents and the predictions of SDM (Fig. 6.9a) and PVDM (Fig. 6.9b) models. It can be observed that both models satisfactorily fitted the experimental data, which were better interpreted by the PVDM model than by the SDM model. It should be noted that the D_s values ranged from 2.43×10^{-10} to 9.7×10^{-10} cm^2/s, whereas the D_{ep} values ranged from 0.85×10^{-7} to 2.91×10^{-7} cm^2/s. On average, D_{ep} values were around 300-fold higher than D_s values, which suggests that TC diffuses within the pores by pore volume diffusion rather than by surface diffusion.

In order to elucidate the mechanism of intraparticle diffusion that governs the diffusion of tetracycline on these adsorbent materials, the experimental data were interpreted with the PVSDM model. This model considers that surface diffusion and pore volume diffusion are both important in the overall adsorption rate. Fig. 6.10a depicts, as an example, the experimental data of TC adsorption rate on sample CR2 and the prediction of the PVSDM model, showing a satisfactory fit of the experimental data. The optimal values of D_{ep} and D_s were 1.73×10^{-7} and 9.7×10^{-11} cm^2/s, respectively. The D_{ep} value obtained with the PVDSM model is very similar to that obtained with the PVDM model ($D_{ep} = 1.94 \times 10^{-7}$ cm^2/s), whereas the D_s value is lower than that obtained with the SDM model.

The relative contribution of pore volume diffusion to the overall intraparticle diffusion was estimated from these results by using the following equation:

$$\frac{N_{AP}}{N_{AS} + N_{AP}} = \frac{D_{ep}\frac{\partial C_{Ar}}{\partial r}}{D_s \rho_p \frac{\partial q}{\partial r} + D_{ep}\frac{\partial C_{Ar}}{\partial r}} \tag{6.19}$$

where N_{AP} and N_{AS} are the mass transport due to the pore volume diffusion and surface diffusion, respectively.

Figure 6.10b shows the relative contribution of pore volume diffusion as a function of time at different dimensionless radial positions $\xi(r/R)$ in sample CR2, as an example; the pore volume contribution always represented more than 84% of the total intraparticle diffusion regardless of the radial position and time. Similar results were obtained for the other adsorbents. These results confirm that

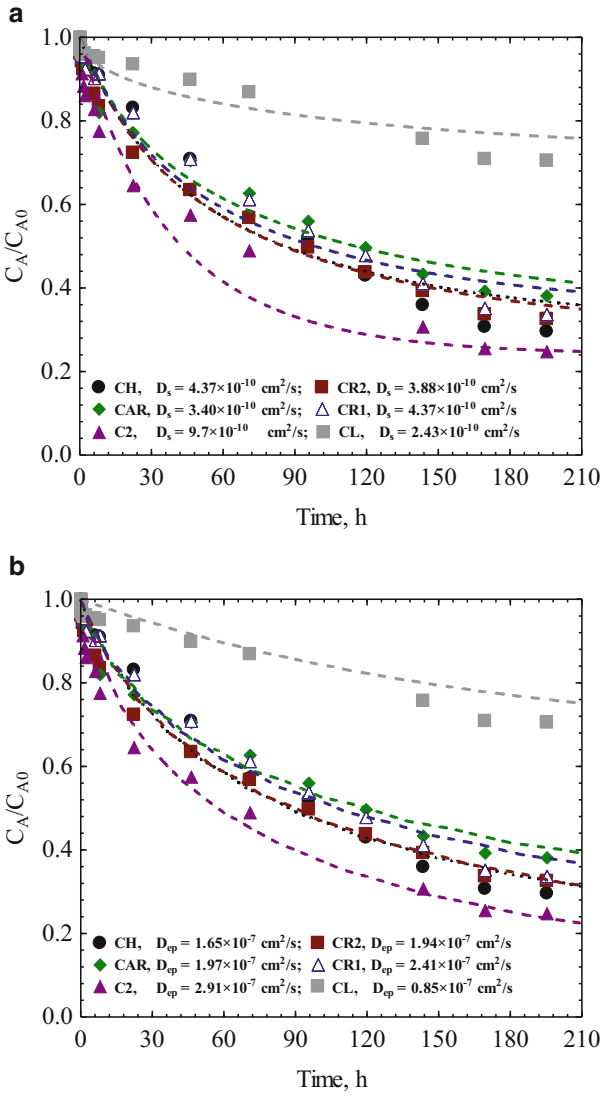

Fig. 6.9 TC adsorption kinetics on the adsorbents. The *lines* represent the prediction of (**a**) SDM model and (**b**) PVDM model. pH = 7, $[TC]_o$ = 700 mg/L, T = 298 K (Ocampo-Pérez et al. 2012)

tetracycline diffusion on adsorbents derived from sewage sludge is governed by pore volume diffusion.

TC molecular diffusion within the adsorbent pores can be drastically affected by the physical properties of the adsorbent, such as the porosity and tortuosity. The porosity of a material is directly related to the total pore volume, while the tortuosity is a function of the pore shape and size distribution. In Fig. 6.11, the D_{ep} values are

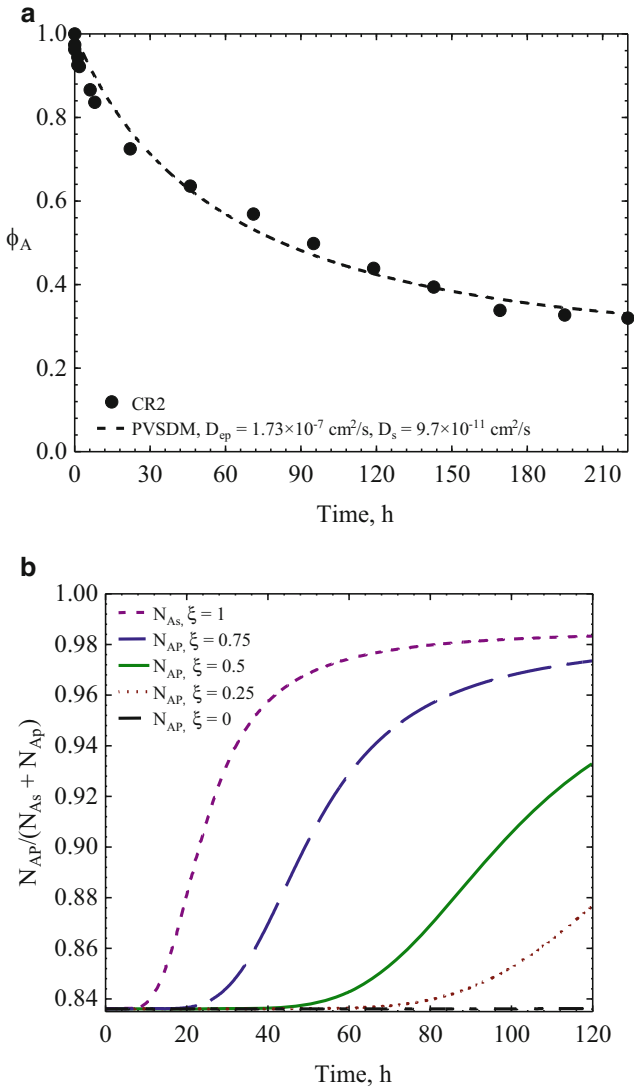

Fig. 6.10 (**a**) TC adsorption kinetics on sample CR2. (**b**) Contribution of pore volume diffusion to the total intraparticle diffusion at different radial positions during TC adsorption on sample CR2 (Ocampo-Pérez et al. 2012)

plotted against the main textural characteristics of the adsorbents (V_2, V_3, $W_0(N_2)$, and S_{ext}). This figure shows a tendency for D_{ep} values to increase with higher V_2, V_3, $W_0(N_2)$, and S_{ext} values. These results indicate that the TC diffusion is directly related to its accessibility to the interior pores. Thus, higher effective pore volume

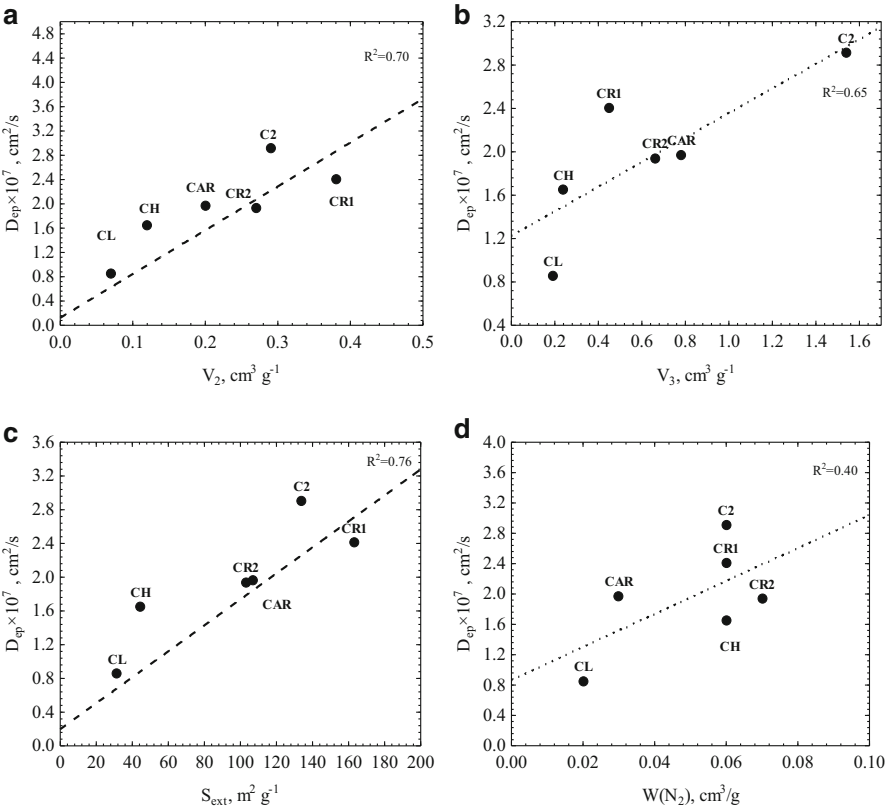

Fig. 6.11 Variation in effective pore volume diffusion coefficients for TC adsorption as a function of textural characteristics of the adsorbents (Ocampo-Pérez et al. 2012)

diffusion coefficients were obtained in the materials with greater macropore and mesopore volumes and, therefore, larger external surface areas.

6.3.3.2 Diffusion of Tetracyclines on Activated Carbon

Activated carbons have unique chemical and textural characteristics which are greatly different to those of adsorbents derived from sewage sludges. For example, CH sample, with the highest S_{BET} value of these adsorbents, has a surface area of 163 m^2/g, which is nearly eight times smaller than that of activated carbon M. Therefore, the diffusion mechanism of tetracyclines on activated carbons could be governed by another kind of driving force different to that corresponding to adsorbents derived from sewage sludges. To analyze this aspect, the TC concentration decay curves for adsorption on S and M activated carbons were predicted

Table 6.17 Mass transfer parameters for the adsorption of TCs on ACs at T = 25 °C, V = 0.1 L and m = 0.1 g (Ocampo-Pérez et al. 2015)

TCs	$D_{AB} \times 10^6$ (cm^2/s)	ACs	$k_L \times 10^7$ (cm/s)	$D_s \times 10^9$ (cm^2/s)
TC	4.87	S	3.0	1.16
		M	2.7	26.0
OTC	4.85	S	3.2	2.60
		M	2.0	2.16
CTC	4.83	S	1.9	0.13
		M	2.4	1.82

with the numerical solution of the PVDM model. The values of D_{ep} were estimated by the tortuosity factor equation as follows:

$$D_{ep} = \frac{D_{AB}\varepsilon_p}{\tau_p} \tag{6.20}$$

where D_{AB} is the molecular diffusion coefficient at infinite dilution (cm^2/s) and τ_p is the tortuosity factor.

As suggested by Leyva-Ramos and Geankoplis (1994), the tortuosity factors for carbons M and S were assumed to be 3.5. The molecular diffusivities of the TCs were calculated using the correlation proposed by Wilke and Chang (1955), and the values are recorded in Table 6.17. From Eq. (6.20), the values of D_{ep} estimated for TC, OTC, and CTC were 6.92×10^{-7}, 6.85×10^{-7}, and 6.72×10^{-7} cm^2/s, respectively. The values of k_L estimated by applying Eq. (6.17) were also included in Table 6.17.

As an example, the rate of adsorption of TC on carbon M was predicted with the PVDM model and using the D_{ep} value estimated by Eq. (6.20). The experimental and the predicted concentration decay curves are depicted in Fig. 6.12. The PVDM considerably overpredicted the concentration decay of TC. This result implies that the rate of adsorption of TC is faster than that predicted with the PVDM. Similar results were observed for the adsorption rates of OTC and CTC on both ACs. These findings suggest that pore volume diffusion is not the only intraparticle diffusion mechanism occurring in the adsorption rate of TCs on activated carbons.

In the PVSDM model, the intraparticle diffusion is assumed to be due to both the pore volume diffusion and surface diffusion. The values of D_{ep} and k_L were estimated as argued earlier. Hence, the surface diffusion coefficient (D_S) was the sole unknown mass transfer parameter and can be calculated by fitting the numerical solution of the PVSDM model to the experimental concentration decay curve data. In this case, the optimal value of D_s was obtained by minimizing the Eq. (6.18).

The concentration decay curve predicted with the PVSDM is plotted in Fig. 6.12 for the adsorption of TC on carbon M. As it can be noted, the PVSDM model satisfactorily fitted the experimental concentration decay data. Similar results were observed for the adsorption rate of the OTC and CTC on both activated carbons. The optimal values of D_s are given in Table 6.17 and increased in the following order:

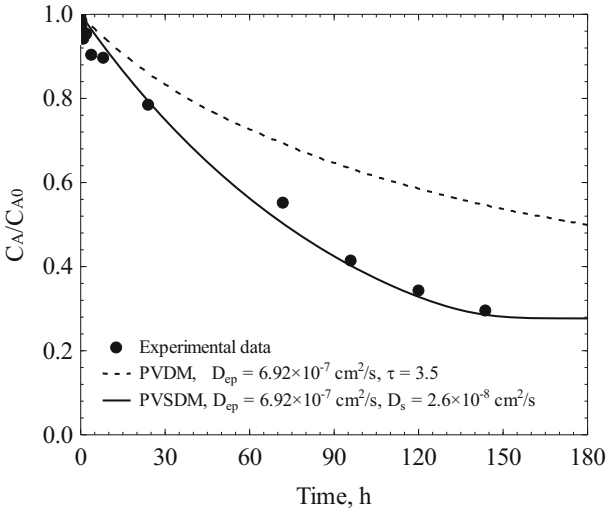

Fig. 6.12 Concentration decay curves of TC for adsorption on carbon M. The *lines* represent the prediction of PVDM and PVSDM models. Initial concentration of TC = 700 mg/L, pH = 4, and T = 298 K (Ocampo-Pérez et al. 2015)

$D_{s,OTC} > D_{s,TC} > D_{s,CTC}$ for carbon S and $D_{s,TC} > D_{s,OTC} > D_{s,CTC}$ for carbon M. The D_s values for carbon M were almost one order of magnitude higher than those for carbon S, except in the case of OTC.

The contribution of each diffusion mechanism to the intraparticle mass transfer of the TCs was estimated by computing the mass flux due to the pore volume diffusion (N_{AP}) and surface diffusion (N_{AS}) using the Eq. (6.19).

Percentage contribution of surface diffusion to the total intraparticle diffusion at various adsorption times and particle radius during TC adsorption on carbon S is depicted in Fig. 6.13. As shown in this figure, the contribution of surface diffusion was markedly dependent on the time and the radial position in the particle. For example, at a time of 33 h, the pore volume diffusion of TC is the main intraparticle diffusion mechanism at the entrance of the pore (750 < particle radius < 800 μm); however, the surface diffusion of TC was almost the only mechanism for particle radius less than 600 μm.

The contribution of pore volume diffusion for carbon S was greater than for carbon M. This result can be explained considering that carbon M has a larger mean micropore size and mesopore, avoiding the influence of restrictive effects at the entrance of pores on the diffusion of TCs.

6.3.3.3 Adsorption Kinetics of Nitroimidazoles on Activated Carbons

The concentration decay curves during the adsorption of DMZ, MNZ, RNZ, and TNZ on commercial activated carbons M, S, and on the sample C-2 from chemical

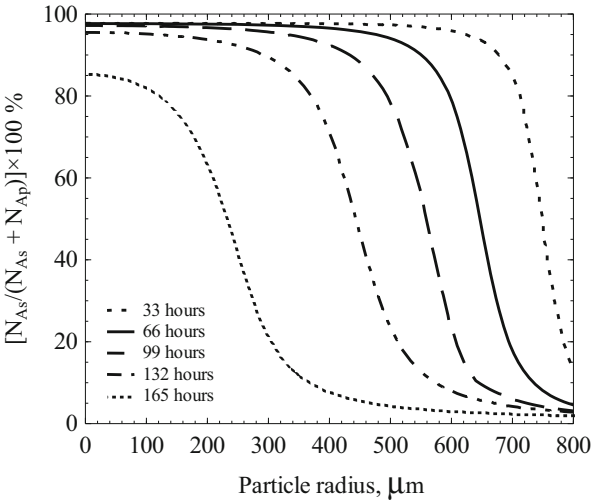

Fig. 6.13 Percentage contribution of surface diffusion to the total intraparticle diffusion at various times and radius during TC adsorption on carbon S (Ocampo-Pérez et al. 2015)

activation of petroleum coke are depicted in Fig. 6.14a–d, respectively. Independently of the nitroimidazole type, the adsorption equilibrium in carbon C-2 was not approached in less than 150 h, and the adsorption equilibrium in carbon M was attained in lesser times than in the other carbons. Hence, the adsorption rate in carbon M was faster than in the other carbons, whereas carbon C-2 presented the slowest adsorption rate.

Independently of the carbon, the MNZ molecule presented the shorter times to reach equilibrium. For example, the approximate times to approach equilibrium in carbon S were 55, 74, 76, and 195 h for MNZ, DMZ, RNZ, and TNZ, respectively. This result indicated that the adsorption rate of MNZ was faster than those of other molecules; however, accordingly to the molecular diffusivities of the nitroimidazoles, the expected decreasing order of the adsorption rate was DMZ > MNZ > RNZ > TNZ.

The values of the rate constants (k_1 and k_2) and the calculated uptake of the nitroimidazoles at equilibrium, $q_e(calc)$, for the four nitroimidazoles, were evaluated by fitting the pseudo-first-order and pseudo-second-order kinetic models to the adsorption kinetic data, q vs. t. The value for the experimental uptake, $q_e(exp)$, corresponds to the amount of nitroimidazole adsorbed at equilibrium has been obtained from Fig. 6.14a–d.

In general, regardless of the model used and the activated carbon, the rate of adsorption on the activated carbons decreases in the order: MNZ > DMZ > RNZ > TNZ. As an example, this behavior is shown in Fig. 6.15. These results may indicate that textural properties of activated carbons are not solely responsible for the adsorption rate of these compounds, since compounds like MNZ are adsorbed faster than smaller compounds, such as DMZ.

The dependence of the rate constants k_1 and k_2 with respect to the chemical and textural properties of the activated carbons was analyzed. In general, no clear

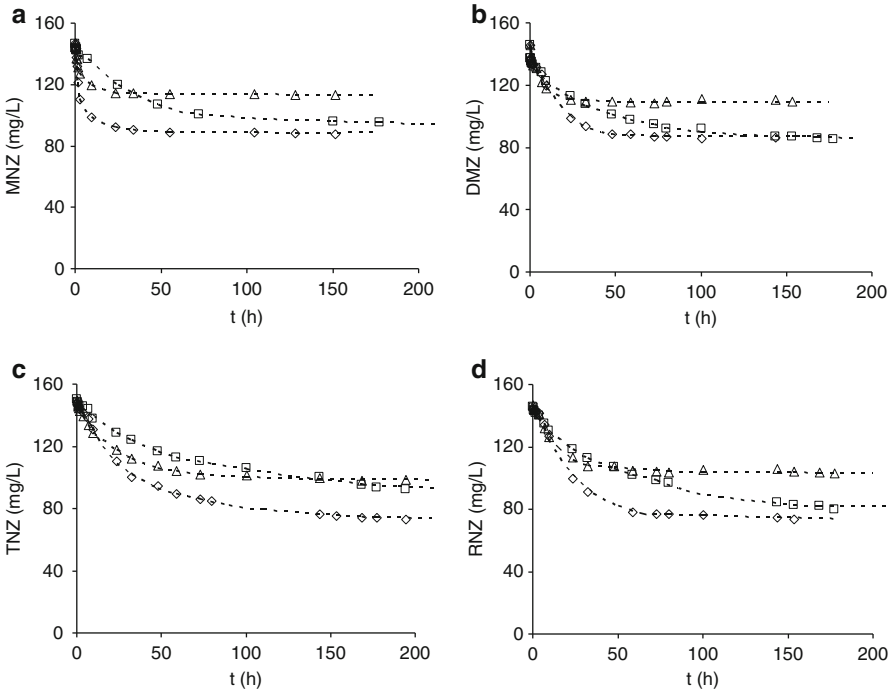

Fig. 6.14 Adsorption kinetics of nitroimidazoles on activated carbons. pH = 7, T = 298 K, [activated carbon] = 0.2 g/L. (◇) S, (Δ) M, (□) C-2. (**a**) $[DMZ]_0$ = 150 mg/L, (**b**) $[MNZ]_0$ = 150 mg/L, (**c**) $[RNZ]_0$ = 150 mg/L, (**d**) $[TNZ]_0$ = 150 mg/L. The *lines* represent the predictions of the pseudo-first-order kinetic model (Méndez-Díaz et al. 2010)

relationship was observed between the pseudo-first- or pseudo-second-order rate constants and the textural properties of the carbons, except that the rate constants k_1 or k_2 are augmented, increasing the micropore volume ($W_0(N_2)$) and mean micropore size ($L_0(N_2)$) of the activated carbon. The relationships between k_1 and $W_0(N_2)$ or $L_0(N_2)$ are depicted in Fig. 6.16a, b for the four nitroimidazoles.

The results plotted in these figures appear to indicate that the adsorption rate k_1 is largely dependent upon the volume and mean micropore size. Nevertheless, meso- and macroporosity do not appear to have a major effect on the adsorption rate in these systems. It is expected that the porous structure does not affect the rate constants of the kinetic models since in these models the diffusion through the pores (intraparticle diffusion) has been neglected, and the surface adsorption in the micropores is the controlling step (Poling et al. 2001; Leyva-Ramos et al. 2009).

The nitroimidazole adsorption rate constant k_1 was also related to surface chemical characteristics of the activated carbons. The kinetic constants (k_1) increased, reducing the oxygen percentage of the activated carbon (Fig. 6.17) and diminishing the content of carbonylic (Fig. 6.18) and phenolic groups (Fig. 6.19). However, the rate constants appeared to be independent upon the other chemical properties of carbon such as the pH_{PZC} or concentration of basic sites. Thus, the

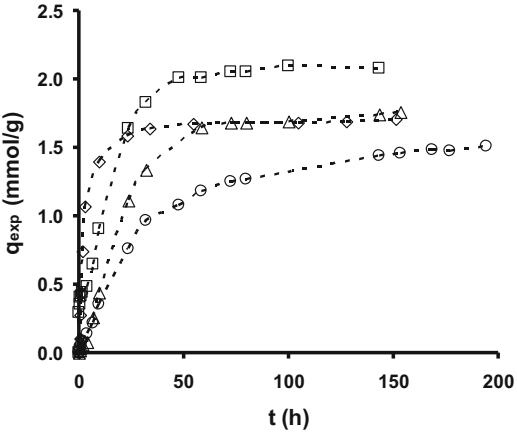

Fig. 6.15 Adsorption kinetics of DMZ, MNZ, RNZ, and TNZ on activated carbon S. pH = 7, [nitroimidazole]$_0$ = 150 mg/L, T = 298 K, [activated carbon] = 0.2 g/L. (□), DMZ; (Δ), MNZ; (◇), RNZ; (○), TNZ. (**- - -**) The *lines* represent the predictions with the pseudo-first-order- (DMZ, MNZ, and RNZ) and pseudo-second-order (TNZ) kinetic models (Méndez-Díaz et al. 2010)

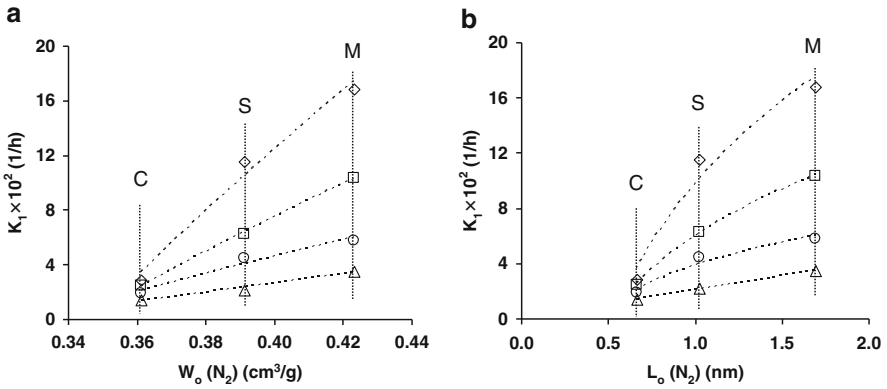

Fig. 6.16 Adsorption rate constants of (◇), MNZ; (□), DMZ; (○), RNZ; (△), TNZ as a function of (**a**) $W_0(N_2)$ and (**b**) $L_0(N_2)$. pH = 7, [NMZ]$_0$ = 150 mg/L, T = 298 K, [activated carbon] = 0.2 g/L (Méndez-Díaz et al. 2010)

adsorption rate constants increased by lessening the oxygen content and carbonylic and phenolic sites in the carbons. This behavior was common to all nitroimidazoles.

The relationships presented in Figs. 6.17, 6.18, and 6.19 indicate that the adsorption rate k_1 is directly related to the carbon hydrophobicity. The carbon hydrophobicity increased, diminishing the oxygen content, and there is a decrease in the competition between water and nitroimidazole molecules for the active adsorption sites of the carbon surface, increasing the adsorption rate of nitroimidazole. Thus, the nitroimidazole adsorption rate constant k_1 can be related

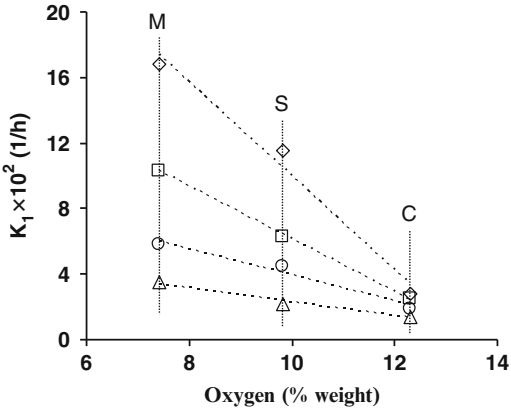

Fig. 6.17 Effect of the activated carbon oxygen content on the nitroimidazole adsorption rate constant. pH = 7, $[\text{nitroimidazole}]_0$ = 150 mg/L, T = 298 K, [activated carbon] = 0.2 g/L. (○), DMZ; (Δ), MNZ; (◇), RNZ; (□), TNZ (Méndez-Díaz et al. 2010)

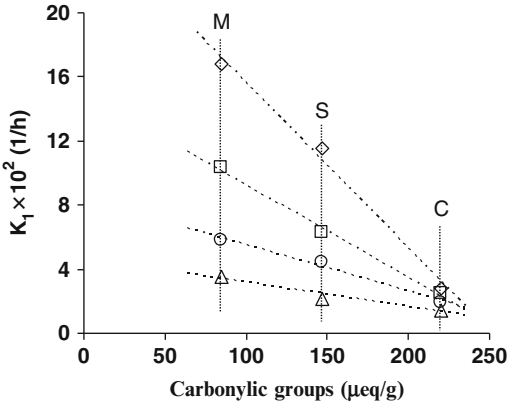

Fig. 6.18 Effect of the carbonylic group content of activated carbons on the nitroimidazole adsorption rate constant. pH = 7, $[\text{nitroimidazole}]_0$ = 150 mg/L, T 298 K, [activated carbon] = 0.2 g/L. (○), DMZ; (Δ), MNZ; (◇), RNZ; (□), TNZ (Méndez-Díaz et al. 2010)

to the relative carbon hydrophobicity as illustrated in Fig. 6.20, and the rate constant k_1 increases with the carbon hydrophobicity.

The adsorption kinetics of nitroimidazoles on activated carbons was also studied by interpreting the experimental kinetic data with the PVDM model. An initial guess of the D_{ep} was calculated using Eq. (6.20) and, assuming a tortuosity factor of τ_p = 3.50, recommended for activated carbons (Leyva-Ramos and Geankoplis 1994; Ocampo-Perez et al. 2011).

The concentration decay data predicted with the diffusional model, as well as the experimental data for the adsorption of DMZ on activated carbon S, are depicted in Fig. 6.21. It can be seen that the diffusional model interpreted satisfactorily well the experimental concentration decay, and the value of τ_p was 3.74 which was very close to τ_p = 3.50, recommended by Leyva-Ramos and Geankoplis (1994).

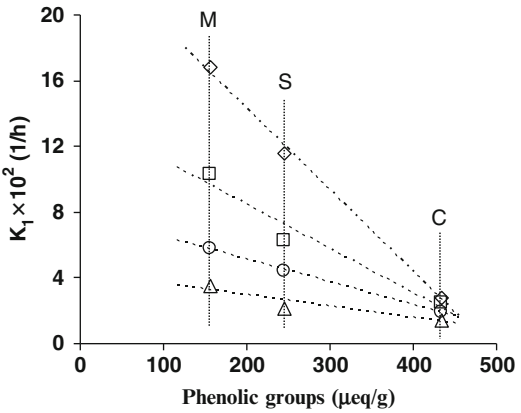

Fig. 6.19 Effect of the phenolic group content of activated carbons on the nitroimidazole adsorption rate constant. pH = 7, $[\text{nitroimidazole}]_0$ = 150 mg/L, T = 298 K, [activated carbon] = 0.2 g/L. (○), DMZ; (Δ), MNZ; (◇), RNZ; (□), TNZ (Méndez-Díaz et al. 2010)

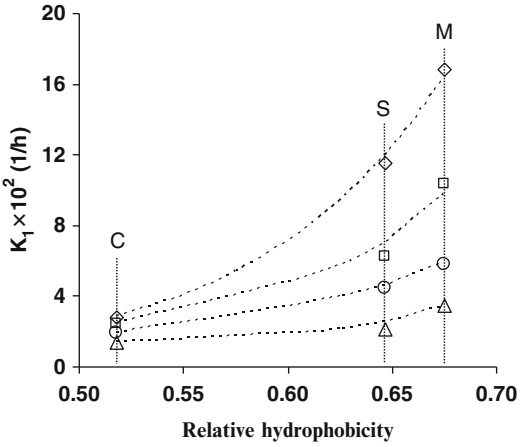

Fig. 6.20 Effect of the activated carbon hydrophobicity on the nitroimidazole adsorption rate constant. pH = 7, $[\text{nitroimidazole}]_0$ = 150 mg/L, T = 298 K, [activated carbon] = 0.2 g/L. (○), DMZ; (Δ), MNZ; (◇), RNZ; (□), TNZ (Méndez-Díaz et al. 2010)

The values of τ_p for RNZ and TNZ varied from 3.84 to 4.91, and these values are within the range of values reported for activated carbons (Leyva-Ramos and Geankoplis 1994; Ocampo-Perez et al. 2011). In general, the diffusional model interpreted well the experimental concentration decay data for the adsorption of RNZ and TNZ on the three carbons. To illustrate the satisfactory fitting obtained with the diffusional model, the predicted and experimental concentration decay data for the adsorption of RNZ on carbon S are plotted in Fig. 6.22. As illustrated in this figure, the diffusional model with $\tau_p = 4.33$ predicted reasonably well the experimental concentration decay curve. In this case the diffusional model with $\tau_p = 3.50$ overpredicted the experimental concentration decay data.

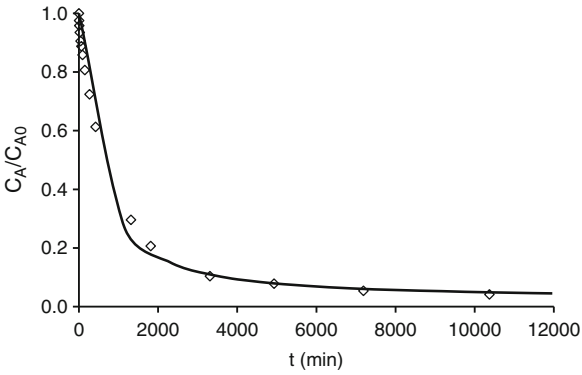

Fig. 6.21 Adsorption kinetics of DMZ on activated carbon S. pH = 7, $[DMZ]_0 = 150$ mg/L, T = 298 K, [activated carbon] = 1 g/L. (◇), experimental data; (—), PVDM model prediction (Méndez-Díaz et al. 2010)

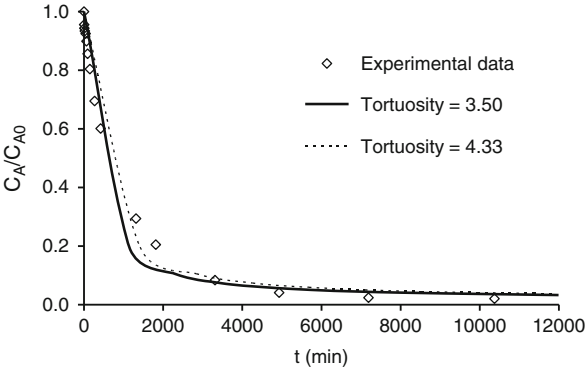

Fig. 6.22 Adsorption kinetics of RNZ on activated carbon S. pH = 7, $[RNZ]_0 = 150$ mg/L, T = 298 K, [activated carbon] = 1 g/L. (◇), experimental data; (—), PVDM model prediction for $\tau_p = 3.5$; (- -), model prediction for $\tau_p = 4.33$ (Méndez-Díaz et al. 2010)

The diffusional model predicted reasonably well the experimental concentration decay data of MNZ during adsorption on the three carbons. As an example, the concentration decay predicted with the diffusional model and the experimental concentration decay for the adsorption of MNZ on carbon S are displayed in Fig. 6.23.

However, the values of τ_p for MNZ range from 1.47 to 2.17. These values are rather smaller than those for the other nitroimidazoles. The concentration decay curve predicted with the diffusional model and $\tau_p = 3.50$ is also graphed in Fig. 6.23, and it can be noticed that the diffusional model with $\tau_p = 3.50$ underpredicted the experimental concentration decay data. This behavior clearly indicates that the tortuosity factor for the adsorption rate of MNZ on carbon S is smaller than $\tau_p = 3.50$.

The low values of τ_p for MNZ can be explained considering that surface diffusion is possibly taking place in the case of the intraparticle diffusion of MNZ. In other words, intraparticle diffusion of MNZ is due to pore volume diffusion as well as surface diffusion. The intraparticle diffusion would be faster when surface diffusion was occurring simultaneously with pore volume diffusion. If surface diffusion was not included in the model such as in this case, this would result in greater values of D_{ep} and smaller values of τ_p.

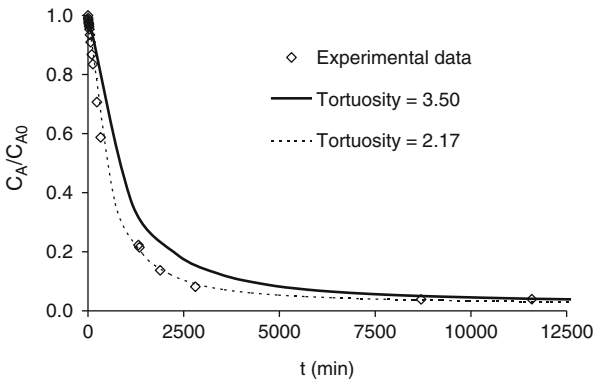

Fig. 6.23 Adsorption kinetics of MNZ on activated carbon S. pH = 7, $[MNZ]_0 = 150$ mg/L, T = 298 K, [activated carbon] = 1 g/L. (◇), experimental data; (—), PVDM model prediction for $\tau_p = 3.5$; (- -), model prediction for $\tau_p = 2.17$ (Méndez-Díaz et al. 2010)

6.4 Adsorption/Biosorption Equilibrium Isotherms of Tetracyclines and Nitroimidazoles on Sludge-Derived Materials and Activated Carbons

6.4.1 Nitroimidazole Adsorption Processes

Both the mechanisms involved in the process of nitroimidazole adsorption and the adsorption capacity of activated carbons were determined by obtaining the corresponding adsorption isotherms. Figure 6.24 depicts, as an example, the normalized adsorption isotherms of the four nitroimidazoles for activated carbon S. It shows the millimoles of nitroimidazole adsorbed per gram of carbon (q_e) versus the equilibrium concentrations normalized for the solubility of each nitroimidazole in water at 298 K (C_{eq}/S_{BET}). Isotherms show the L form of the Giles classification (Giles et al. 1974a, b; Moreno-Castilla 2004), suggesting that the aromatic rings of nitroimidazole molecules are adsorbed in parallel to the carbon surface and that there is no major competition between nitroimidazoles and water molecules for the active adsorption centers on the carbon.

Langmuir (Eq. (6.21)) and Freundlich (Eq. (6.22)) models were applied to the experimental adsorption isotherm data. As stated in Chap. 2, they are the most widely used models for describing this type of process and are represented mathematically as:

$$q_e = \frac{K q_m C_{eq}}{1 + K C_{eq}} \tag{6.21}$$

$$q_e = K_f C_{eq}^{1/n} \tag{6.22}$$

where q_m is the adsorption capacity (mg/g), C_{eq} is the concentration of adsorbate at equilibrium (mg/L), K is the Langmuir constant, K_f is the Freundlich's affinity parameter, and n is the exponential Freundlich's coefficient.

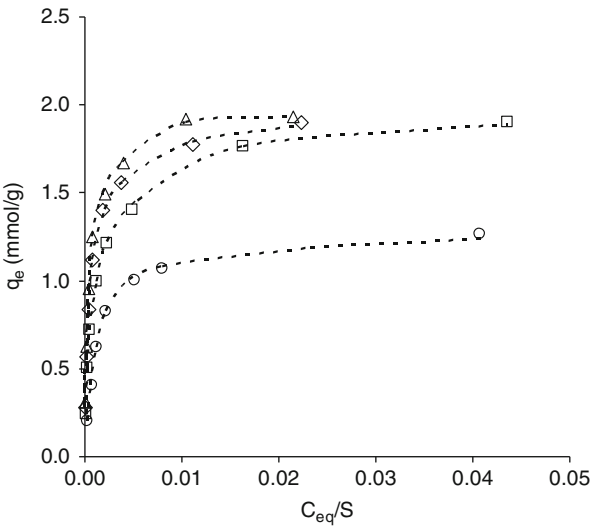

Fig. 6.24 Adsorption isotherms of nitroimidazoles on carbon S. (◇), MNZ; (△), DMZ; (○), TNZ; (□), RNZ. pH = 7, T = 298 K (Rivera-Utrilla et al. 2009)

The determination coefficients obtained were >0.99 for all systems with the Langmuir equation (Table 6.18) but ranged from 0.842 for the TNZ-carbon S system to 0.987 for DMZ-carbon M when the Freundlich equation was applied (Table 6.19). Although both models served to explain our results, the Langmuir model fitted better the experimental data.

The adsorption capacity was very elevated for all carbons and nitroimidazoles (Table 6.18), with q_m values ranging from 1.04 mmol/g for TNZ-carbon C-2 to 2.04 mmol/g for DMZ-carbon C-2. In general, relative affinity values, Kq_m, were also higher than those usually reported in aromatic compound adsorption (Radovic et al. 2001), indicating the high chemical affinity of nitroimidazoles for carbon. Interestingly, the constant K value in Langmuir's equation (related to adsorption energy) increased in the order DMZ < MNZ < RNZ < TNZ, which may be related to the solubility of these nitroimidazoles in water, with an increase in their adsorption energy as solubility decreases (Table 6.15). The corresponding values of the Freundlich exponential coefficient, $1/n$, were low, ranging from 0.214 to 0.295 (Table 6.19), which also indicates strong adsorbent-adsorbate interactions (Freundlich 1926).

The adsorption capacity of carbon for the different nitroimidazoles was expressed per unit of carbon surface area (q'_m) to enable comparisons among them (Table 6.18). Except in the case of TNZ, the adsorption capacity of carbon increased in the order M < S < C-2, which may be related to the oxygen content of carbon, which increased in the same direction. Thus, in the case of carbon C-2 and S, this oxygen is mainly forming phenolic groups, which are electronic activators of the aromatic rings of carbon graphene planes; this favors the adsorption of aromatic compounds like nitroimidazoles, which can be adsorbed by dispersion interactions of π electrons of their aromatic rings with π electrons of

Table 6.18 Parameters obtained by applying Langmuir's equation to the adsorption isotherms of nitroimidazoles on activated carbons S, M, and C-2 (Rivera-Utrilla et al. 2009)

	q_m (mmol/g)			$q'_m\ 10^3$ (mmol/m^2)			K (L/mmol)			Kq_m (L/g)		
Nitroimidazole	S	*M*	*C*-2	S	*M*	*C*-2	S	*M*	*C*-2	S	*M*	*C*-2
MNZ	1.92	1.25	1.68	1.56	0.96	1.98	52.11	9.44	23.50	100.00	11.82	39.37
DMZ	1.99	1.32	2.04	1.62	1.01	2.40	43.84	9.38	23.29	87.24	12.39	47.62
TNZ	1.37	1.56	1.04	1.12	1.20	1.23	75.79	94.24	56.45	104.17	147.06	58.82
RNZ	1.97	1.82	1.89	1.61	1.40	2.23	52.85	25.49	24.57	104.11	46.51	46.51

Table 6.19 Parameters obtained by applying Freundlich's equation to the adsorption isotherms of nitroimidazoles on activated carbons S, M, and C-2 (Rivera-Utrilla et al. 2009)

	S			M			C-2		
Nitroimidazole	1/n	K_f (L/g)	R^2	1/n	K_f (L/g)	R^2	1/n	K_f (L/g)	R^2
MNZ	0.247	403.27	0.925	0.268	171.67	0.968	0.282	248.42	0.932
DMZ	0.235	408.97	0.901	0.261	191.20	0.987	0.260	345.46	0.893
TNZ	0.295	268.47	0.842	0.214	439.44	0.915	0.280	200.26	0.885
RNZ	0.223	479.40	0.935	0.262	317.03	0.967	0.240	361.80	0.928

the carbon graphene planes (Radovic et al. 2001; Moreno-Castilla 2004). Furthermore, the presence of oxygen in the carbon favors the establishment of hydrogen bonds between nitroimidazoles and the carbon surface. These bonds may be responsible for the strong adsorbent-adsorbate interactions detected in these systems and commented above.

Comparison of the adsorption capacity of carbon for each nitroimidazole (q'_m) shows that, with the exception of carbon M, q'_m decreased in the order DMZ > RNZ > MNZ > TNZ. These results show some relationship with the size of the nitroimidazole molecules and hence with their accessibility to the carbon porosity. Thus, TNZ has the largest molecule size and was the least adsorbed, whereas DMZ has the smallest molecule size and therefore highest accessibility to the carbon surface and showed the highest adsorption. Besides the accessibility of nitroimidazoles to the carbon surface, the electronic density of their aromatic ring also increases their adsorption, since it enhances the abovementioned π-π adsorbate-adsorbent dispersion interactions. Based on the chemical composition of these nitroimidazoles and the electronic activating/deactivating power of the groups they contain, the electronic density of aromatic rings decreases in the order DMZ > RNZ ≈ MNZ > TNZ, the same order found for the increase in adsorption capacity of these nitroimidazoles. These results demonstrate that the adsorption process is mainly determined by the adsorbent-adsorbate dispersion interactions described above.

6.4.2 *Tetracyclines Adsorption Isotherms*

Table 6.20 exhibits the data obtained by applying Langmuir and Freundlich equations to the adsorption isotherms of TCs on activated carbons M and S. In all systems, they yielded determination coefficients close to unity. Although both models could be used to explain the results, in general, the Langmuir model best fits the experimental data.

The results in Table 6.20 indicate that, regardless of the carbon and TC considered, the adsorption capacity of the activated carbons was very high, with q_m values ranging from 471.1 mg/g for the TC-carbon M system to 65.1 mg/g for the CTC-S

system. In general, the values of relative affinity (Kq_m) were relatively high, indicating the high chemical affinity of the TCs for the carbons. The corresponding values of Freundlich's exponential coefficient ($1/n$) were low, ranging from 0.10 to 0.52, indicating strong adsorbent-adsorbate interactions. All of these results demonstrate the high effectiveness of these commercial activated carbons for TC removal from water.

As shown in Table 6.20, the capacity of carbon M to adsorb the three TCs was higher than that of carbon S, and its relative affinity with these adsorbates was also considerably superior. For both carbons, the capacity to adsorb these TCs increased in the order CTC < OTC < TC.

Radovic et al. (2001) in their extensive review of the literature on organic compound adsorption on carbons concluded that the adsorption mechanism of these processes remains controversial. They reported that both electrostatic and dispersive adsorbent-adsorbate interactions are involved in the adsorption of aromatic compounds. Coughlin and Ezra (1968) suggested that the adsorption of aromatic compounds on activated carbon is based on the establishment of dispersion interactions between π electrons of the organic compound aromatic ring and π electrons of the activated carbon graphene planes (π-π interactions). Furthermore, Leon and Leon et al. (1992) found that basic carbons ($pH_{PZC} > 7$) with a low oxygen percentage are characterized by a high content of electron-rich sites in their graphene planes and a low concentration of surface electron-attracting oxygen groups, which could enhance the adsorption of aromatic compounds according to the mechanism proposed by Coughlin and Ezra (1968).

Given that TC molecules have neutral charge at the study pH (4–5), Figure 6.4b, electrostatic interactions between positively charged activated carbon surface and TC molecules are weak, and the adsorption mechanism must be largely governed by dispersive adsorbent-adsorbate interactions (Rivera-Utrilla and Sánchez-Polo 2002). Consequently, the greater adsorption capacity of carbon M is partly due to its lower oxygen content and hence higher hydrophobicity. The chemical composition of the TCs and the electron activating/deactivating power of their functional groups means that the electron density of the aromatic ring decreases in the order TC > OTC > CTC, the same order as found for their capacity for adsorption. These results demonstrate that the adsorption process is mainly governed by

Table 6.20 Results obtained from applying Langmuir and Freundlich equations to the TC adsorption isotherms (Rivera-Utrilla et al. 2013a)

TCs	Carbon	Langmuir			Freundlich		
		R^2	q_m (mg/g)	Kq_m (L/g)	R^2	1/n	K (mg/g) (L/mg)
TC	S	0.9998	375.4	52.0	0.9939	0.17	178
	M	0.9999	471.1	142.0	0.9851	0.10	263
OTC	S	0.9911	252.6	6.1	0.9912	0.45	19
	M	0.9991	413.2	15.0	0.9782	0.23	100
CTC	S	0.9535	65.1	4.2	0.9939	0.52	3
	M	0.9984	309.9	10.0	0.9893	0.21	86

dispersive interactions. In addition, the establishment of hydrogen bonds between the phenolic groups of TCs and the oxygenated groups of carbon would also contribute to the high adsorption of these pollutants.

A further aspect to be considered in adsorption is the accessibility of the adsorbate to the activated carbon surface, which is determined by the adsorbate molecule size and carbon pore dimensions. Thus, the higher adsorption capacity of carbon M is partly due to its larger mean micropore size and mesopore volume (Table 6.1), giving TCs greater access to its pores and presenting a larger surface fraction that is effective in adsorption in comparison to carbon S. As stated above, the adsorption capacity of carbons for these TCs shows that it decreases in the order TC > OTC > CTC. These results are in part related to the size of TC molecules (Table 6.14) and their consequent accessibility to the carbon porosity. Thus, the tetracycline with largest molecule size (CTC) shows the lowest adsorption and the one with the smallest size (TC) the highest.

Table 6.21 shows that sludge-derived adsorbents had a higher capacity to adsorb TC in comparison to the commercial activated carbons used in the present study (Table 6.20) and other adsorbent reported in the literature (Pils and Laird 2007; Wang et al. 2010; Zou et al. 2012; Chang et al. 2012; Zhou et al. 2012; Liu et al. 2012, 2013; Huang et al. 2013; Li et al. 2013; Liao et al. 2013; Lin et al. 2013), reaching a value of 672.0 mg/g for the C2 sample. Taking into account the small surface area and low C content of these materials, their high TC adsorption capacity can only be explained by the formation of complexes between TC and the metal elements present in these samples. The formation of chelate-type coordination compounds between TC and metal elements has been extensively studied in the literature (Figueroa et al. 2004; Jones et al. 2005; Başakçilardan-Kabakci et al. 2007). Thus, a characteristic chemical property of TCs is their capacity to form insoluble chelates at neutral pH with certain metal ions, such as Fe^{2+}, Al^{3+}, Ca^{2+}, and Mg^{2+} (Van der Bijl and Pitigoi-Aron 1995; Carson and Breslyn 1996; Chakrawarti 2001; Wang et al. 2008a). Therefore, the presence of these metal cations in our adsorbents (Table 6.10) would explain their high adsorption capacity.

6.4.3 Influence of Operational Variables

6.4.3.1 Influence of Solution pH

Figure 6.25 depicts, as an example, the influence of solution pH on TC adsorption on activated carbon M, showing a pH range from 2 to 7 at which the amount adsorbed remains constant, with a reduction in adsorption at higher pH values. This behavior was observed for all three TCs studied, maintaining the adsorption order TC > OTC > CTC observed for the adsorption isotherms. A similar behavior was detected for carbon S, except that adsorption was reduced from pH values of around 9.

Table 6.21 Results of applying Langmuir equation to tetracycline adsorption isotherms of adsorbents obtained from sludge and others from literature (Rivera-Utrilla et al. 2013a)

Adsorbent	Langmuir			References
	R^2	q_m (mg/g)	Kq_m (L/g)	
C2	0.9988	672.0	10.96	In this work
CR2	0.9898	593.4	7.64	In this work
CH	0.9966	553.3	6.23	In this work
CAR	0.9979	512.1	4.70	In this work
HCl-modified Zeolite	0.9998	20.4	7.29	Zou et al. (2012)
Magnetic resin (Q100)[a]	0.9292	429.7	13.42	Zhou et al. (2012)
Alkali biochar	0.9570	58.82	0.882	Liu et al. (2012)
MCM-41 impregnated with zeolite[b]	0.9811	419.3	3.04	Liu et al. (2013)
Graphene oxide functionalized magnetic particles	0.9920	39.1	17.6	Lin et al. (2013)
Anaerobic granular sludge[a]	0.9910	4.61	–	Li et al. (2013)
Bamboo charcoal	0.9211	22.7	0.454	Liao et al. (2013)
Activated carbon fiber modified by microwave	0.9818	312	13.54	Huang et al. (2013)
Illite	0.988	32	–	Chang et al. (2012)
Clays, humic substances, and clay-humic complexes[a]	–	12	–	Pils and Laird (2007)
The red soil (RS, UdicFerrosols)	–	12	–	Wang et al. (2010)

[a]T = 45 °C
[b]T = 50 °C

The behavior depicted in Fig. 6.25 is due to the progressive ionization of the surface oxygenated groups of the activated carbon with higher solution pH, which produces an increase in its negative surface charge density and a consequent reduction in adsorption. This is because repulsive electrostatic interactions are established between the carbon surface, negatively charged at pH values above its pH_{PZC}, and the TC molecules, negatively charged at pH values above their pK_{a2} values. These results indicate that, depending on the solution pH, electrostatic adsorbent-adsorbate interactions also play an important role in these adsorption processes.

Regarding nitroimidazoles, Fig. 6.26 shows, as an example, the influence of solution pH on nitroimidazole adsorption of activated carbon M. The solution pH did not significantly affect the process of adsorption of nitroimidazoles on carbon M between pH 4 and 11, but all four nitroimidazoles showed a slight decrease at pH 2. According to their pK_{a1} values (Table 6.15 and Fig. 6.5), this is because of the protonation of nitroimidazoles at pH values close to 2. As a result, repulsive electrostatic interactions are established between the carbon surface, positively

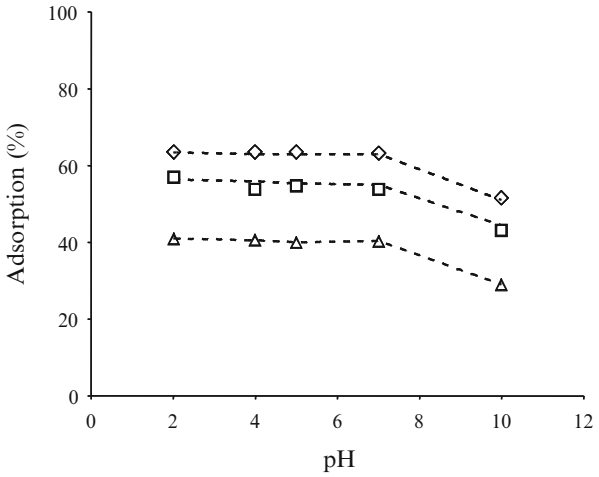

Fig. 6.25 Amount of TCs adsorbed on M carbon, at equilibrium-8 days, as a function of solution pH. (◊), TC; (□), OTC; (△), CTC. T = 298 K. [M] = 1 g/L. $[TCs]_0$ = 700 mg/L (Rivera-Utrilla et al. 2013a)

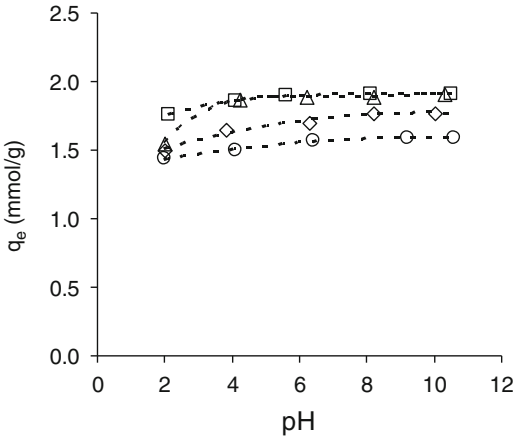

Fig. 6.26 Influence of pH in nitroimidazole adsorption process on carbon M. (◇), MNZ; (△), DMZ; (○), TNZ; (□), RNZ. T = 298 K. [M] = 1 g/L. $[nitroimidazole]_o$ = 600 mg/L (Rivera-Utrilla et al. 2009)

charged at pH 2 ($pH_{solution} < pH_{PZC}$) and the nitroimidazoles, positively charged at pH values close to 2. Similar results were observed for the other carbon samples.

Results depicted in Fig. 6.26 verify that electrostatic interactions do not play a major role in the adsorption of nitroimidazoles on activated carbon surface between pH 4 and 11, since nitroimidazole molecules are neutral under these conditions, and surface oxygenated groups of the activated carbon progressively ionize with higher solution pH. Therefore, the increase in negative surface charge does not produce a reduction in the adsorption of the contaminants. These data confirm that non-electrostatic interactions are largely responsible for the adsorption of these compounds on activated carbon, as reported in the above section.

6.4.3.2 Influence of Solution Ionic Strength

Figure 6.27 depicts, as an example, the results for TC adsorption on carbon M in the presence of increasing NaCl concentrations. Ionic strength can affect the adsorption process on activated carbons. According to the results obtained by López-Ramón et al. (2003), the presence of electrolytes in solution can modify the strength of adsorbate-adsorbent electrostatic interactions. These interactions, either attractive or repulsive, can be increased or reduced by varying the solution ion strength.

Figure 6.27 shows that, with an increase in NaCl concentration, in the medium from 0.0 to 0.1 molar, the adsorption percentage is reduced by around 20%, which remains constant at higher NaCl concentrations. These results can be explained by considering that electrostatic interactions between the carbon surface and adsorbate are attractive at the study pH (7), because the carbon surface is positively charged but the TC molecules are partially ionized (Figure 6.4b). Therefore, adsorption capacity is decreased with greater ion strength due to a possible screening effect of the carbon surface charge produced by the added NaCl, i.e., by placing Cl^- and Na^+ ions between carbon surface and TC molecules, reducing attractive electrostatic interactions between carbon surface and the fraction of ionized TC. A similar behavior was found for the rest of tetracyclines (Rivera-Utrilla et al. 2013a). In the case of nitroimidazole adsorption, the effect of solution ionic strength was less marked (Rivera-Utrilla et al. 2009).

6.4.3.3 Influence of the Presence of Microorganisms

The presence of microorganisms in natural water and wastewater may exert a considerable influence on the effectiveness of activated carbon because microorganisms can be adsorbed on the carbon during water treatment, giving rise to the

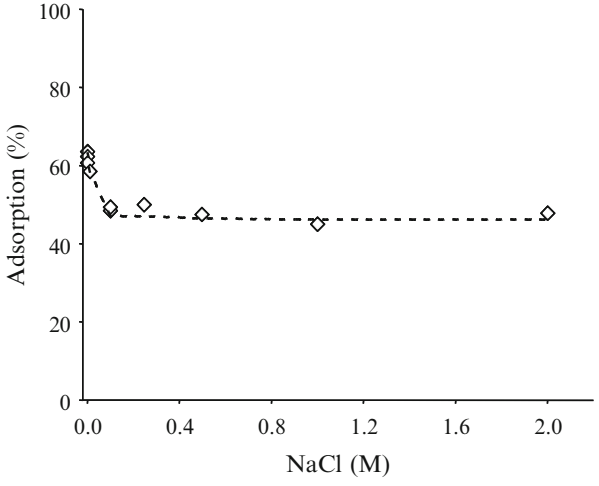

Fig. 6.27 Adsorption of TC on carbon M as a function of solution ionic strength. pH = 7, T = 298 K. [M] = 1 g/L. $[TC]_0$ = 700 mg/L (Rivera-Utrilla et al. 2013a)

formation of bacteria colonies and the consequent modification of the chemical and textural characteristics of the carbon surface (Rivera-Utrilla et al. 2001, 2003; Moreno-Castilla et al. 2003a; Bautista-Toledo et al. 2008).

This aspect was analyzed by obtaining TC and CTC adsorption isotherms on carbon M in the presence of bacteria from secondary effluents of a wastewater treatment plant. Figure 6.28 depicts the adsorption/biosorption isotherms of TC and CTC on carbon M in the presence and the absence of these bacteria. Table 6.22 shows the results of applying Langmuir's equation to these isotherms.

The effect of the adsorption of bacteria on the chemical and textural properties of activated carbon was previously reported by our research group (Rivera-Utrilla et al. 2001, 2003), finding (i) a decrease in the surface area due to pore blocking and (ii) a reduction in the pH_{PZC}, which increases the negative surface charge density of the activated carbon. Moreover, given that the external walls of bacteria are formed by phospholipids (Nikaido and Vaara 1985), their adsorption on activated carbon (Fig. 6.29) increases the hydrophobicity of the carbon surface.

The results obtained (Table 6.22) show that the presence of microorganisms during the adsorption of both TCs decreases the adsorption capacity of the activated carbon and reduces the adsorbate-adsorbent relative affinity values (Kq_m) by around 80% and 30% for TC and CTC, respectively. This behavior may be due to two factors: (i) an increase in electrostatic repulsions between the ionized TC fraction and the activated carbon surface, which are both negatively charged at the study pH, and (ii) the appearance of exopolymers released by bacteria outside the cell in the presence of the TC (Fig. 6.29c). These exopolymers are mainly formed by lipids and carbohydrates (Beech et al. 1999; Sheng et al. 2005) which form a biofilm (see Fig. 6.29) that reduces the activated carbon surface area accessible to the TC molecules and hence the amount adsorbed.

In the case of nitroimidazoles, Fig. 6.30 depicts the adsorption/biosorption isotherms of DMZ and RNZ on carbon S in the presence and absence of microorganisms. Application of Langmuir's equation to these isotherms (Table 6.23) showed, unlike what was found in the case of TCs, that the presence of microorganisms during the adsorption of these nitroimidazoles increases the adsorption capacity of carbon S by 22% and decreased the adsorbate-adsorbent relative affinity values (Kq_m) by around 60%. These results suggest that the presence of bacteria produces a change in the main interactions responsible for the adsorption and may therefore affect the adsorption mechanism. Nitroimidazole biodegradation kinetics by the bacteria under study were investigated before obtaining the biosorption isotherms, observing no biodegradation of these compounds under the experimental conditions used. Thus, results shown in Fig. 6.30 and Table 6.23 may be explained by the increase in the hydrophobicity of the activated carbon surface, which is known to considerably favor the adsorption process. All these results indicate that the effect of the presence of microorganisms on the adsorption process depends on the adsorbate-adsorbent system.

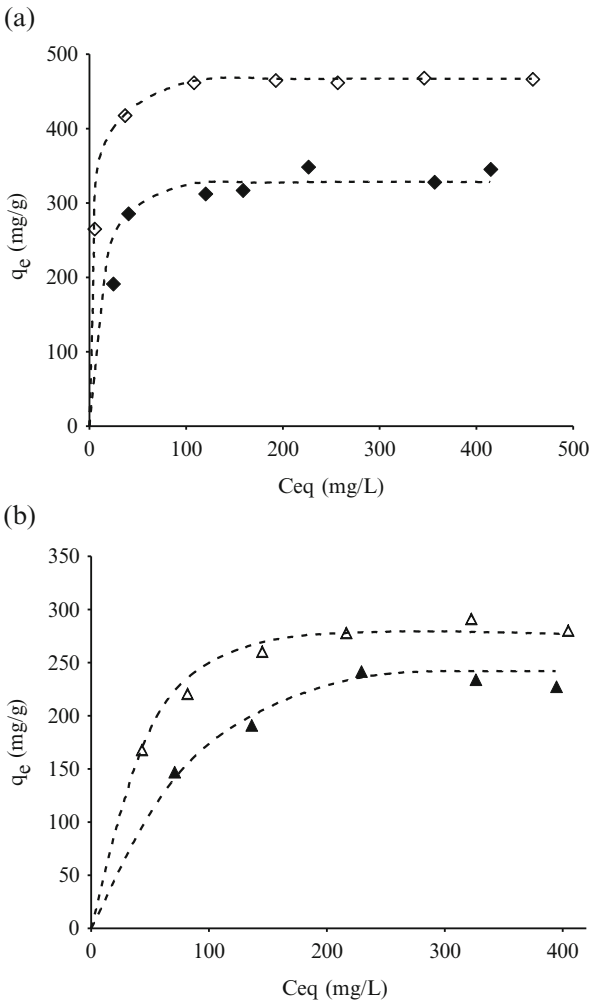

Fig. 6.28 Adsorption isotherms of TC (**a**) and CTC (**b**) on carbon M in the presence (♦, ▲) and absence (◇, △) of bacteria. pH = 7, T = 298 K. [M] = 1 g/L (Rivera-Utrilla et al. 2013a)

Table 6.22 Results of applying Langmuir's equation on TC and CTC adsorption isotherms of M carbon in the presence and absence of microorganisms (Rivera-Utrilla et al. 2013a)

	With bacteria		Without bacteria	
Tetracycline	q_m (mg/g)	Kq_m (L/g)	q_m (mg/g)	Kq_m (L/g)
TC	353.33	24.36	471.18	142.17
OTC	261.42	6.15	309.99	10.22

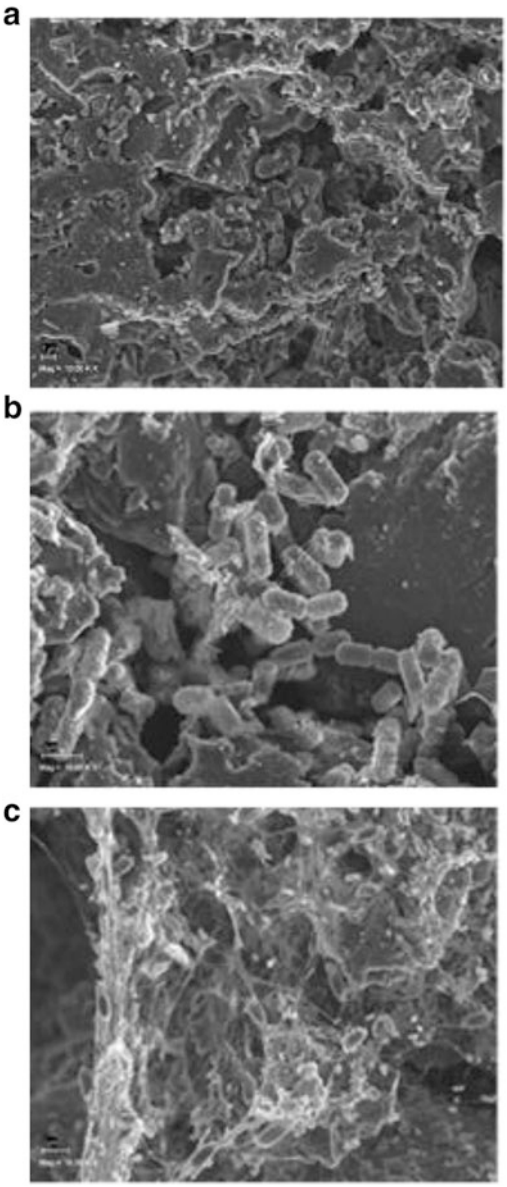

Fig. 6.29 SEM images of carbon M before and after TC biosorption. (**a**) Carbon M, (**b**) carbon M + bacteria, (**c**) carbon M + bacteria + TC (Rivera-Utrilla et al. 2013a)

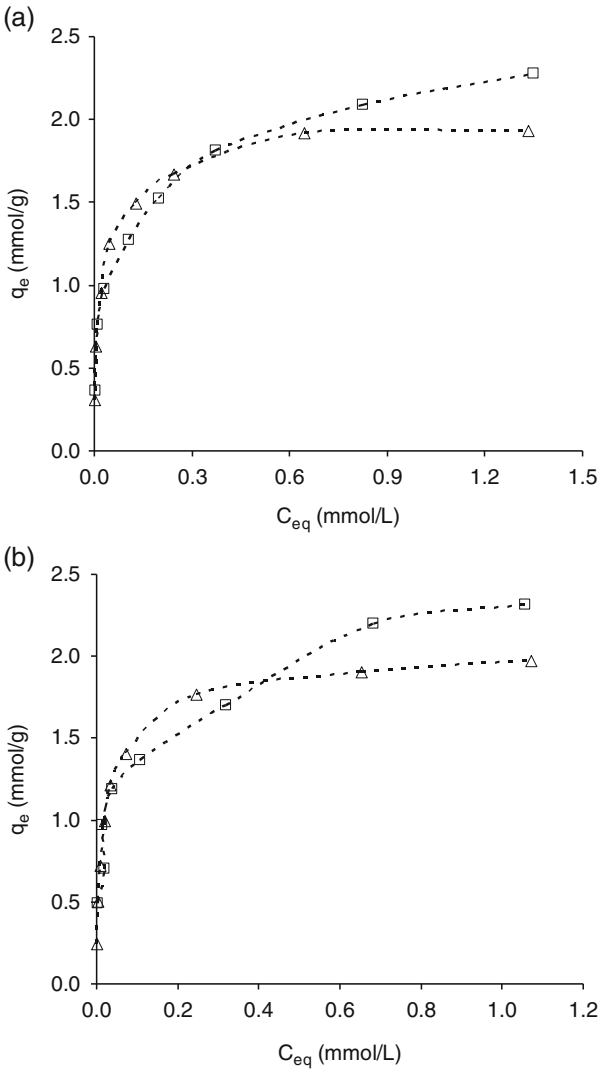

Fig. 6.30 Adsorption isotherms of DMZ (**a**) and RNZ (**b**) in the presence (□) and absence (△) of microorganisms on carbon S. pH = 7, T = 298 K (Rivera-Utrilla et al. 2009)

Table 6.23 Results obtained by applying Langmuir's equation to the adsorption isotherms of DMZ and RNZ on carbon S in the presence and absence of microorganisms (Rivera-Utrilla et al. 2009)

DMZ				RNZ			
With bacteria		Without bacteria		With bacteria		Without bacteria	
q_m (mmol/g)	Kq_m (L/g)	q_m (mmol/g)	Kq_m (L/g)	q_m (mmol/g)	Kq_m (L/g)	q_m (mmol/g)	Kq_m (L/g)
2.44	31.06	1.99	87.24	2.42	44.25	1.97	104.11

6.5 Adsorption of Tetracyclines and Nitroimidazoles on Sludge-Derived Materials and Activated Carbons in Dynamic Regime. Determination of the Breakthrough Curves and Characteristics of the Adsorbent Columns

TC and TNZ adsorption was also studied in dynamic regime, constantly passing a TC (20 mg/L) or TNZ (100 mg/L) solution through adsorbent columns (2 g, height 7 cm, diameter 1 cm, packing density 0.36 g/cm^3) at a flow of 1.5 mL/min and obtaining both the bed breakthrough curves up to 0.9 breakthrough and the bed characteristics. Fig. 6.31 shows the column breakthrough curves for TC adsorption on CR2, CH, CAR, and M samples. The adsorbent sample obtained from sludge in the presence of a phenolic resin (CR2) allows a larger volume of TC-contaminated water to be treated in comparison to the samples obtained in the presence of humic acid (CH) or clayey soil (CAR). Nevertheless, the water volume treated by the commercial activated carbon M sample is around threefold higher than the volume treated by sample CR2.

Based on the column breakthrough curves, a previously reported method (Zogorski and Faust 1977; Ferro-García et al. 1990) was used to determine the column characteristics listed in Table 6.24, showing that the TC amount adsorbed at the breakthrough point ($q_{0.02}$) was very low, especially in sludge-derived samples. Regardless of the adsorbent sample considered, the amount adsorbed at column breakthrough point ($q_{0.02}$) was lower than the adsorption capacity observed in static regime (Tables 6.20 and 6.21). These results indicate that adsorption is much less effective in dynamic than static regime due to problems of TC diffusion into the adsorbent pores and the shorter contact time between adsorbate and adsorbent.

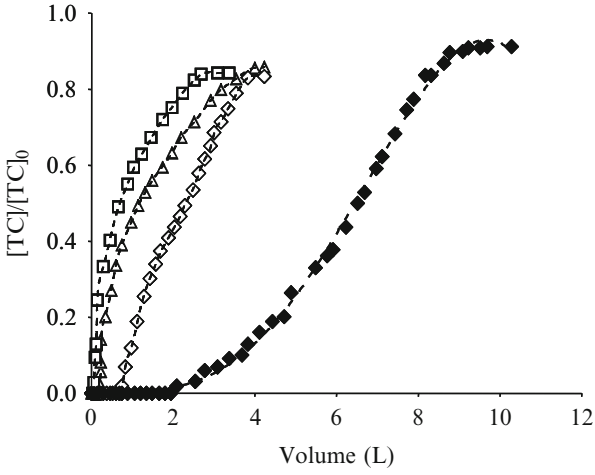

Fig. 6.31 Breakthrough curves for TC adsorption on sludge-derived adsorbents and activated carbon M. (♦), M; (◊), CR2; (Δ), CAR; (□), CH. T = 25 °C, pH = 7, $[TC]_0$ = 20 mg/L (Rivera-Utrilla et al. 2013a)

Table 6.24 Characteristics of the TC adsorption columns (Rivera-Utrilla et al. 2013a)

Adsorbent	$q_{0.02}$ (mg/g)	$q_{0.80}$ (mg/g)	$V_{0.02}$ (L)	Φ	H_{MTZ} (cm)	Gu (%)
CH	0.7	21	0.07	0.32	18.59	19.93
CR2	7.5	28	0.75	0.54	8.01	39.24
CAR	2.0	29	0.21	0.43	12.80	20.55
M	21.0	60	2.10	0.65	6.53	44.97

$X_{0.02}$ is the amount of TC adsorbed at column breakthrough point. $X_{0.80}$ is the amount adsorbed on the column when TC concentration in the effluent is 80% of the initial concentration. $V_{0.02}$ is the volume treated at column breakthrough point. Φ is the fractional capacity of the mass transference zone. H_{MTZ} is the height of the mass transference zone. Gu is the grade of utility of the column

Table 6.25 Characteristics of carbon M columns in TC adsorption as a function of the type of water used (Rivera-Utrilla et al. 2013a)

Water	$q_{0.02}$ (mg/g)	$q_{0.80}$ (mg/g)	$V_{0.02}$ (L)	Φ	H_{MTZ} (cm)	Gu (%)
Ultrapure	21	60	2.10	0.65	6.53	44.97
Surface	5	49	0.50	0.45	10.87	22.03
Groundwater	15	51	1.50	0.50	8.26	37.46
Wastewater	2	26	0.20	0.41	11.91	19.43

The amount of TC adsorbed at the column breakthrough point was higher for the adsorbent bound with phenolic resin than for the other samples obtained with different binding agents. Moreover, the height of the mass transference zone of this CR2 column was smaller and its utility grade (Gu) higher, indicating that it is the most effective sludge sample column to remove TC from water. Nevertheless, these sludge-derived materials are not appropriate for column adsorption processes, mainly because of their low compaction capacity. Hence, according to these results, these materials can mainly be used for adsorption in static regime (conventional batch technique).

TC adsorption in dynamic regime was also studied using columns of activated carbon M and water with different chemical compositions, in an attempt to reproduce as far as possible the real hypothetic situation by using surface water, groundwater, and wastewater. Table 6.25 shows the column characteristics obtained from the corresponding breakthrough curves. We highlight the differences in column characteristics as a function of the type of water used. As shown in Table 6.25, $V_{0.02}$, $q_{0.02}$, and the Gu values were lower in surface water and, especially, wastewater than in ultrapure water, and the height of the mass transference zone was greater. This is because the adsorbent porosity is partially blocked by adsorption of the organic matter present in natural waters, reducing the surface area available for TC molecule adsorption and markedly decreasing the treatment effectiveness. This reduction in effectiveness is accentuated by competition

between the organic matter and the TC molecules for adsorbent surface adsorption sites, in agreement with previous reports (Carter et al. 1992; Kilduff and Wigton 1999).

Figure 6.32 depicts the breakthrough curves for TNZ adsorption on columns of activated carbon M in different types of water. In all types of water, the amount adsorbed at the breakthrough point of the column ($q_{0.02}$) was lower than the amount adsorbed in static regime. As mentioned above, this less effective adsorption in dynamic versus static regime can be attributed to problems of TNZ diffusion to the interior of carbon pores. The differences in the values of the column characteristics as a function of the chemical composition of the different waters were analyzed. Unlike the results obtained for tetracycline, $V_{0.02}$ and $q_{0.02}$ values and the degree of utility of the column (Gu) were higher in surface water and especially in groundwater than in ultrapure water (Table 6.26), and the height of the mass transference zone was lower in the former waters, indicating an increase in the effectiveness of the treatment. Two effects may explain these findings: (i) lower solubility of nitroimidazoles in surface and groundwater as a consequence of their higher alkalinity and salinity, since nonpolar organic compounds are known to markedly decrease their solubility in the presence of salts (West and Harwell 1992; Flaming et al. 2003), explaining the increase in $V_{0.02}$, $q_{0.02}$, and Gu, and (ii) the presence of Ca^{2+} ions may modify the adsorption of organic molecules on activated carbon,

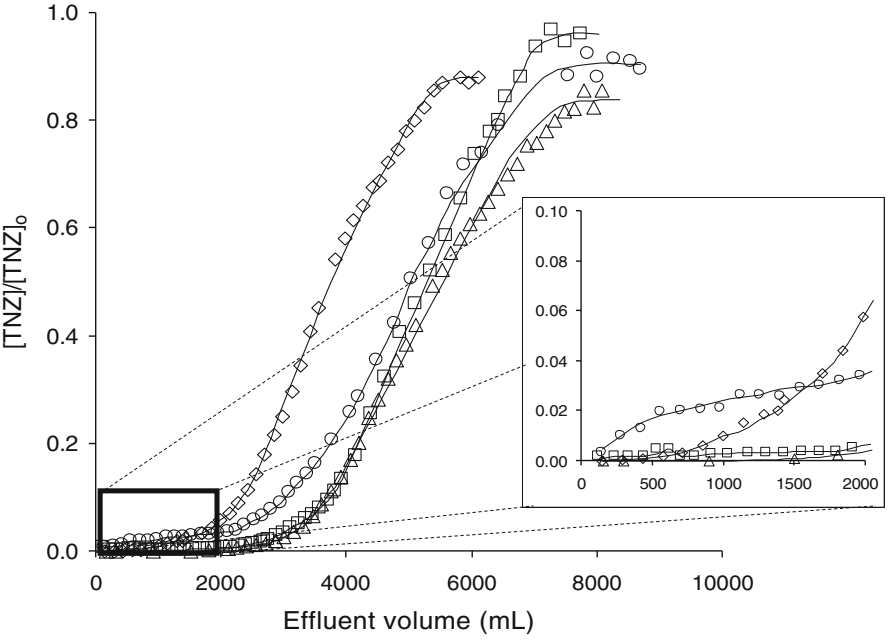

Fig. 6.32 Breakthrough curves of TNZ on carbon M as a function of the type of water used. (◇), ultrapure water; (□), surface; (△), groundwater; (○), wastewater. T = 298 K. $[\text{nitroimidazole}]_o$ = 100 mg/L (Rivera-Utrilla et al. 2009)

Table 6.26 Characteristics of carbon M columns in the adsorption of TNZ as a function of the type of water used (Rivera-Utrilla et al. 2009)

Water	$q_{0.02}$ (mmol/g)	$V_{0.02}$ (mL)	Φ	H_{MTZ} (cm)	Gu (%)
Ultrapure	0.35	1377	0.636	6.044	41.14
Surface	0.64	2693	0.660	4.341	56.13
Groundwater	0.73	2870	0.591	4.697	57.50
Waste	0.17	700	0.694	7.670	15.77

since this ion can react as a co-adsorbate by creating a bridge between the structure of activated carbon and adsorbed molecules (Lafrance and Mazet 1989; Cannon et al. 1994).

Markedly lower $V_{0.02}$, $q_{0.02}$, and Gu values and a higher H_{MTZ} value were obtained for TNZ adsorption in wastewaters, because adsorption of dissolved organic matter on carbon surface would reduce the surface area available for the adsorption of TNZ molecules. The effectiveness of treatment would be reduced by the competition between dissolved organic matter and TNZ molecules for active sites on the activated carbon, as previously reported (Carter et al. 1992; Kilduff and Wigton 1999). Similar values for the fractional capacity of the mass transference zone (Φ) were observed in all water samples studied (Table 6.26).

The results presented in Table 6.26 and Fig. 6.32 are very interesting from an application point of view. Thus, according to the results obtained, nitroimidazoles could be efficiently removed from surface and groundwater by adsorption on activated carbon; however, due to the high concentration of organic carbon dissolved in wastewater, activated carbon adsorption would not be the best technological alternative to remove nitroimidazoles from wastewater.

6.6 Conclusions

Sludge chemical activation considerably increases the adsorption capacity of sludge for tetracyclines. The addition of a binding agent (humic acid, phenolic resin, or clayey soil) before chemical activation of the material slightly reduces this adsorption capacity but improves its granulometry and allows the production of large granules, enhancing their technological applicability and, therefore, their commercialization. The capacity of all sludge adsorbents to adsorb tetracyclines is much higher than that of a commercial activated carbon (Merck) widely used in water treatment.

Petroleum coke was chemically activated with KOH. The activation process considerably develops the micro-, meso-, and macroporosity of the raw material. The surface chemical nature of the original coke was also modified by the activation process, increasing its surface basicity.

Experimental data for TC concentration decay curves on the treatment sludge-derived adsorbents are adequately interpreted by the kinetic and diffusion models applied. The pseudo first-order kinetic model provides the best interpretation of TC

adsorption kinetics on all adsorbents under study, and their rate constants vary in a linear manner with their macro- and mesopore volumes and decrease with the carboxylic group content. The intraparticle diffusion model demonstrated that the TC adsorption rate on all adsorbents is controlled by intraparticle diffusion. Pore volume diffusion represents more than 80% of the total intraparticle diffusion, indicating that surface diffusion does not play a major role in TC diffusion on these adsorbents.

The concentration decay data of the TCs during the adsorption was interpreted quite well using the PVSDM model, and it was demonstrated that the pore volume diffusion and surface diffusion are important in the adsorption rate of the TC_S. The contribution of surface diffusion is directly related to the adsorption capacity of the activated carbons. In general, the higher the adsorption capacity, the greater is the contribution of surface diffusion.

The adsorption rates of the nitroimidazoles DMZ, MNZ, RNZ, or TNZ on activated carbons were better interpreted by a pseudo-first-order model or a pseudo-second-order model depending on the adsorbate-adsorbent system studied. The adsorption rate of the nitroimidazoles decreases in the order MNZ > DMZ > RNZ > TNZ. Therefore, in the case of MNZ, molecular size does not appear to be a determining factor in the adsorption rate. The adsorption rate of nitroimidazoles is related to the decrease in oxygen percentage of activated carbons and, therefore, their increase in hydrophobicity. Thus, hydrophobic interactions appear to favor the kinetics of the adsorption process. A diffusional model was applied that combines external mass transfer and intraparticle diffusion, achieving an adequate fit to the experimental data in the majority of the systems studied.

The TC adsorption capacity of the sludge-derived materials is very high (512–672 mg/g) and greater than that of the commercial activated carbons studied, attributable to the strong tendency of TCs to form complex ions with some of the metal ions in these materials.

The commercial activated carbons studied have a high TC adsorption capacity (65–471 mg/g). At the study pH (pH 4–5), the capacity of carbons to adsorb TCs is directly related to the density of delocalized π electrons in both the graphene layers of the carbon and the TC aromatic ring.

The solution pH and the presence of electrolytes had a major influence on TC adsorption on the commercial activated carbons, indicating that electrostatic adsorbent-adsorbate interactions also play an important role in TC adsorption at pH values that produce TC deprotonation. However, in the case of nitroimidazoles, the pH of the medium and the concentration of the electrolyte present do not have a major effect on the adsorption of these compounds on activated carbon, indicating that adsorbent-adsorbate electrostatic interactions do not play an important role in these adsorption processes.

The presence of bacteria in solution reduced TC adsorption/biosorption on the commercial activated carbons, weakening interactions between the adsorbate and the biofilm formed on the carbon surface. These results are explained by the formation of exopolymers released by bacteria in the presence of

TC. Nitroimidazoles are not degraded by the microorganisms used in the biological treatment stage of a wastewater treatment plant. However, the presence of these microorganisms during the adsorption of these compounds increases their adsorption/biosorption on the activated carbon, although interactions between adsorbate and carbon surface are weakened.

TC adsorption on both sludge-derived materials and activated carbons was markedly lower in dynamic versus static regime, attributable to problems of TC diffusion into the adsorbent pores and the shorter contact time between adsorbent and adsorbate in the case of dynamic regime. The extend of TC adsorption was markedly lower in natural waters (surface water, groundwater, and wastewater) than in ultrapure water, which may be explained by the reduced adsorbent surface area available for TC adsorption due to the adsorption of dissolved organic matter in these type of water. Nevertheless, in the case of nitroimidazoles, results obtained in dynamic regime show that the adsorption capacity of the activated carbon was markedly higher in surface and groundwater than in ultrapure water and urban wastewaters.

References

Adler NE, Koschorreck J, Rechenberg B (2008) Environmental impact assessment and control of pharmaceuticals: the role of environmental agencies. Water Sci Technol 57:91–97

Ahmed MJ, Theydan SK (2013) Microporous activated carbon from Siris seed pods by microwave-induced KOH activation for metronidazole adsorption. J Anal Appl Pyrol 99:101–109

Al-Ahmad A, Daschner FD, Kümmerer K (1999) Biodegradability of cefotiam, ciprofloxacin, meropenem, penicillin G, and sulfamethoxazole and inhibition of waste water bacteria. Arch Environ Con Tox 37:158–163

Ayscough NJ, Fawell J, Franklin G (2000) Review of human pharmaceuticals in the environment. Environment Agency, Bristol

Başakçilardan-Kabakci S, Thompson A, Cartmell E, Le Corre K (2007) Adsorption and precipitation of tetracycline with struvite. Water Environ Res 79:2551–2556

Batt AL, Kim S, Aga DS (2007) Comparison of the occurrence of antibiotics in four full-scale wastewater treatment plants with varying designs and operations. Chemosphere 68:428–435

Bautista-Toledo MI, Méndez-Díaz JD, Sánchez-Polo M, Rivera-Utrilla J, Ferro-García MA (2008) Adsorption of sodium dodecylbenzenesulfonate on activated carbons: effects of solution chemistry and presence of bacteria. J Colloid Interf Sci 317:11–17

Beech I, Hanjagsit L, Kalaji M, Neal AL, Zinkevich V (1999) Chemical and structural characterization of exopolymers produced by Pseudomonas sp NCIMB 2021 in continuous culture. Microbiology 145:1491–1497

Beita-Sandí W, Ersan MS, Uzun H, Karanfil T (2016) Removal of N-nitrosodimethylamine precursors with powdered activated carbon adsorption. Water Res 88:711–718

Bendesky A, Menéndez D, Ostrosky-Wegman P (2002) Is metronidazole carcinogenic? Mutat Res-Rev Mutat 511:133–144

Benk A (2010) Utilisation of the binders prepared from coal tar pitch and phenolic resins for the production metallurgical quality briquettes from coke breeze and the study of their high temperature carbonization behaviour. Fuel Process Technol 91:1152–1161

Blanchard G, Maunaye M, Martin G (1984) Removal of heavy metals from waters by means of natural zeolites. Water Res 18:1501–1507

Calamari D (2002) Assessment of persistent and bioaccumulating chemicals in the aquatic environment. Toxicology 181:183–186

Calisto V, Ferreira CI, Oliveira JA, Otero M, Esteves VI (2015) Adsorptive removal of pharmaceuticals from water by commercial and waste-based carbons. J Environ Manag 152:83–90

Campbell HW (2000) Sludge management–future issues and trends. Water Sci Technol 41:1–8

Cannon FS, Snoeyink VL, Lee RG, Dagois G (1994) Reaction mechanism of calcium-catalyzed thermal regeneration of spent granular activated carbón. Carbon 32:1285–1301

Carballa M, Omil F, Lema JM, Llompart M, Garcia-Jares C, Rodriguez I, Gómez M, Ternes TM (2004) Behavior of pharmaceuticals, cosmetics and hormones in a sewage treatment plant. Water Res 38:2918–2926

Carrales-Alvarado DH, Ocampo-Pérez R, Leyva-Ramos R, Rivera-Utrilla J (2014) Removal of the antibiotic metronidazole by adsorption on various carbon materials from aqueous phase. J Colloid Interf Sci 436:276–285

Carson MC, Breslyn W (1996) Simultaneous determination of multiple tetracycline residues in milk by metal chelate affinity chromatography: collaborative study. J AOAC Int 79:29–42

Carter MC, Weber WJ Jr, Olmstead KP (1992) Effects of background dissolved organic matter on TCE adsorption by GAC. J Am Water Works Ass 84:81–91

Cavdar AD, Kalaycioglu H, Hiziroglu S (2008) Some of the properties of oriented strandboard manufactured using kraft lignin phenolic resin. J Mater Process Tech 202:559–563

Chakrawarti PB (2001) Chelation and antibiotic activity. J Ind Chem Soc 78:273–279

Chang P, Li Z, Jean J, Jiang W, Wang C, Lin K (2012) Adsorption of tetracycline on 2:1 layered non-swelling clay mineral illite. Appl Clay Sci 67–68:158–163

Choi KJ, Kim SG, Kim S (2008) Removal of tetracycline and sulfonamide classes of antibiotic compound by powdered activated carbon. Environ Technol 29:333–342

Cooper ER, Siewicki TC, Phillips K (2008) Preliminary risk assessment database and risk ranking of pharmaceuticals in the environment. Sci Total Environ 398:26–33

Correa M, Laza JM, Vilas JL, Bilbao E, Rodríguez M, León LM (2010) Reutilization of thermostable polyester wastes by means of agglomeration with phenolic resins. Waste Manag 30:2305–2311

Coughlin RW, Ezra FS (1968) Role of surface acidity in the adsorption of organic pollutants on the surface of carbon. Environ Sci Technol 2:291–297

Dias JM, Alvim-Ferraz MCM, Almeida MF, Rivera-Utrilla J, Sánchez-Polo M (2007) Waste materials for activated carbon preparation and its use in aqueous-phase treatment: a review. J Environ Manag 85:833–846

Ferro-García MA, Carrasco-Marín F, Rivera-Utrilla J, Utrera-Hidalgo E, Moreno-Castilla C (1990) The use of activated carbon columns for the removal of ortho-phosphate ions from aqueous solutions. Carbon 28:91–95

Figueroa RA, Leonard A, Mackay AA (2004) Modeling tetracycline antibiotic sorption to clays. Environ Sci Technol 38:476–483

Flaming JE, Knox RC, Sabatini DA, Kibbey TC (2003) Surfactant effects on residual water and oil saturations in porous media. Vadose Zone J 2:168–176

Freundlich H (1926) Colloid and capillary chemistry. Metheun, London

Ganguly SK, Goswami AN (1996) Surface diffusion kinetics in the adsorption of acetic acid on activated carbon. Separ Sci Technol 31:1267–1278

Gao Y, Li Y, Zhang L, Huang H, Hu J, Shah SM, Su X (2012a) Adsorption and removal of tetracycline antibiotics from aqueous solution by graphene oxide. J Colloid Interf Sci 368:540–546

Gao P, Mao D, Luo Y, Wang L, Xu B, Xu L (2012b) Occurrence of sulfonamide and tetracycline-resistant bacteria and resistance genes in aquaculture environment. Water Res 46:2355–2364

Garrido J, Linares-Solano A, Martin-Martinez JM, Molina-Sabio M, Rodriguez-Reinoso F, Torregrosa R (1987) Use of nitrogen vs. carbon dioxide in the characterization of activated carbons. Langmuir 3:76–81

Giles CH, Smith D, Huitson A (1974a) A general treatment and classification of the solute adsorption isotherm I Theoretical. J Colloid Interf Sci 47:755–765

Giles CH, D'Silva AP, Easton IA (1974b) A general treatment and classification of the solute adsorption isotherm part II Experimental interpretation. J Colloid Interf Sci 47:766–778

Gómez-Pacheco CV, Rivera-Utrilla J, Sánchez-Polo M, López-Peñalver JJ (2012) Optimization of the preparation process of biological sludge adsorbents for application in water treatment. J Hazard Mater 217:76–84

Gu C, Karthikeyan KG (2008) Sorption of the antibiotic tetracycline to humic-mineral complexes. J Environ Qual 37:704–711

Halling-Sørensen B, Nielsen SN, Lanzky PF, Ingerslev F, Lützhøft HH, Jørgensen SE (1998) Occurrence, fate and effects of pharmaceutical substances in the environment-A review. Chemosphere 36:357–393

Ho YS, Mckay G (1998) Kinetic models for the sorption of dye from aqueous solution by wood. Process Saf Environ 76:183–191

Huang L, Shi C, Zhang B, Niu S, Gao B (2013) Characterization of activated carbon fiber by microwave heating and the adsorption of tetracycline antibiotics. Separ Sci Technol 48:1356–1363

Hunter WG, Hunter JS (1978) Statistics for experimenters: an introduction to design, data analysis, and model building. Wiley, New York, p 319

Ip AW, Barford JP, McKay G (2010) A comparative study on the kinetics and mechanisms of removal of Reactive Black 5 by adsorption onto activated carbons and bone char. Chem Eng J 157:434–442

Jones AD, Bruland GL, Agrawal SG, Vasudevan D (2005) Factors influencing the sorption of oxytetracycline to soils. Environ Toxicol Chem 24:761–770

Kang HY, Park SS, Rim YS (2006) Preparation of activated carbon from paper mill sludge by KOH-activation. Korean J Chem Eng 23:948–953

Kilduff JE, Wigton A (1999) Sorption of TCE by humic-preloaded activated carbon: incorporating size- exclusion and pore blockage phenomena in a competitive adsorption model. Environ Sci Technol 33:250–256

Kulshrestha P, Giese RF Jr, Aga DS (2004) Investigating the molecular interactions of oxytetracycline in clay and organic matter: insights on factors affecting its mobility in soil. Environ Sci Technol 38:4097–4105

Kümmerer K (2001) Drugs in the environment: emission of drugs, diagnostic aids and disinfectants into wastewater by hospitals in relation to other sources–a review. Chemosphere 45:957–969

Kümmerer K (ed) (2008) Pharmaceuticals in the environment: sources, fate, effects and risks. Springer Science Business Media, Berlin/Heidelberg, pp 73–93

Kümmerer K, Al-Ahmad A, Mersch-Sundermann V (2000) Biodegradability of some antibiotics, elimination of the genotoxicity and affection of wastewater bacteria in a simple test. Chemosphere 40:701–710

Lafrance P, Mazet M (1989) Adsorption of humic substances in the presence of sodium salts. J Am Water Works Ass 81:155–162

Lau AH, Lam NP, Piscitelli SC, Wilkes L, Danziger LH (1992) Clinical pharmacokinetics of metronidazole and other nitroimidazole anti-infectives. Clin Pharmacokinet 23:328–364

Leon y Leon CA, Solar JM, Calemma V, Radovic LR (1992) Evidence for the protonation of basal plane sites on carbon. Carbon 30:797–811

Leyva-Ramos R, Geankoplis CJ (1985) Model simulation and analysis of surface diffusion in liquids in porous solids. Chem Eng Sci 40:799–807

Leyva-Ramos R, Geankoplis CJ (1994) Diffusion in liquid-filled pores of activated carbon I Pore volume diffusion. Can J Chem Eng 72:262–271

Leyva-Ramos R, Rivera-Utrilla J, Medellín-Castillo NA, Sánchez-Polo M (2009) Kinetic modelling of naphthalenesulphonic acid adsorption from aqueous solution onto untreated and ozonated activated carbons. Adsorpt Sci Technol 27:395–411

Li K, Ji F, Liu Y, Tong Z, Zhan X, Hu Z (2013) Adsorption removal of tetracycline from aqueous solution by anaerobic granular sludge: equilibrium and kinetic studies. Water Sci Technol 67:1490–1496

Liao P, Zhan Z, Dai J, Wu X, Zhang W, Wang K, Yuan S (2013) Adsorption of tetracycline and chloramphenicol in aqueous solutions by bamboo charcoal: a batch and fixed-bed column study. Chem Eng J 228:496–505

Lin AYC, Yu TH, Lateef SK (2009) Removal of pharmaceuticals in secondary wastewater treatment processes in Taiwan. J Hazard Mater 167:1163–1169

Lin Y, Xu S, Li J (2013) Fast and highly efficient tetracyclines removal from environmental waters by graphene oxide functionalized magnetic particles. Chem Eng J 225:679–685

Lindberg R, Jarnheimer PÅ, Olsen B, Johansson M, Tysklind M (2004) Determination of antibiotic substances in hospital sewage water using solid phase extraction and liquid chromatography/mass spectrometry and group analogue internal standards. Chemosphere 57:1479–1488

Liu P, Liu W, Jiang H, Chen J, Li W, Yu H (2012) Modification of bio-char derived from fast pyrolysis of biomass and its application in removal of tetracycline from aqueous solution. Bioresour Technol 121:235–240

Liu M, Hou L, Yu S, Xi B, Zhao Y, Xia X (2013) MCM-41 impregnated with A zeolite precursor: synthesis, characterization and tetracycline antibiotics removal from aqueous solution. Chem Eng J 223:678–687

López-Ramón V, Moreno-Castilla C, Rivera-Utrilla J, Radovic LR (2003) Ionic strength effects in aqueous phase adsorption of metal ions on activated carbons. Carbon 41:2020–2022

Marsh H, Yan DS, O'Grady TM, Wennerberg A (1984) Formation of active carbons from cokes using potassium hydroxide. Carbon 22:603–611

Mathers JJ, Flick SC, Cox LA (2011) Longer-duration uses of tetracyclines and penicillins in US food-producing animals: indications and microbiologic effects. Environ Int 37:991–1004

Méndez A, Gascó G, Freitas MMA, Siebielec G, Stuczynski T, Figueiredo JL (2005) Preparation of carbon-based adsorbents from pyrolysis and air activation of sewage sludges. Chem Eng J 108:169–177

Méndez-Díaz JD, Prados-Joya G, Rivera-Utrilla J, Leyva-Ramos R, Sánchez-Polo M, Ferro-García MA, Medellín-Castillo NA (2010) Kinetic study of the adsorption of nitroimidazole antibiotics on activated carbons in aqueous phase. J Colloid Interf Sci 345:481–490

Misra DN (1991) Adsorption and orientation of tetracycline on hydroxyapatite. Calcified Tissue Int 48:362–367

Moreno-Castilla C (2004) Adsorption of organic molecules from aqueous solutions on carbon materials. Carbon 42:83–94

Moreno-Castilla C, Bautista-Toledo I, Ferro-García MA, Rivera-Utrilla J (2003a) Influence of support surface properties on activity of bacteria immobilised on activated carbons for water denitrification. Carbon 41:1743–1749

Moreno-Castilla C, Perez-Cadenas AF, Maldonado-Hodar FJ, Carrasco-Marın F, Fierro JLG (2003b) Influence of carbon–oxygen surface complexes on the surface acidity of tungsten oxide catalysts supported on activated carbons. Carbon 41:1157–1167

Nikaido H, Vaara M (1985) Molecular basis of bacterial outer membrane permeability. Microbiol Rev 49:1–32

Ocampo-Perez R, Leyva-Ramos R, Alonso-Davila P, Rivera-Utrilla J, Sanchez-Polo M (2010) Modeling adsorption rate of pyridine onto granular activated carbon. Chem Eng J 165:133–141

Ocampo-Perez R, Leyva-Ramos R, Mendoza-Barron J, Guerrero-Coronado RM (2011) Adsorption rate of phenol from aqueous solution onto organobentonite: surface diffusion and kinetic models. J Colloid Interf Sci 364:195–204

Ocampo-Pérez R, Rivera-Utrilla J, Gómez-Pacheco C, Sánchez-Polo M, López-Peñalver JJ (2012) Kinetic study of tetracycline adsorption on sludge-derived adsorbents in aqueous phase. Chem Eng J 213:88–96

Ocampo-Pérez R, Orellana-Garcia F, Sánchez-Polo M, Rivera-Utrilla J, Velo-Gala I, López-Ramón MV, Alvarez-Merino MA (2013) Nitroimidazoles adsorption on activated carbon cloth from aqueous solution. J Colloid Interf Sci 401:116–124

Ocampo-Pérez R, Leyva-Ramos R, Rivera-Utrilla J, Flores-Cano JV, Sánchez-Polo M (2015) Modeling adsorption rate of tetracyclines on activated carbons from aqueous phase. Chem Eng Res Des 104:579–588

Oleszkiewicz JA, Mavinic DS (2001) Wastewater biosolids: an overview of processing, treatment, and management. Can J Civil Eng 28:102–114

Otowa T, Tanibata R, Itoh M (1993) Production and adsorption characteristics of MAXSORB: high-surface-area active carbon. Gas Sep Purif 7:241–245

Otowa T, Nojima Y, Miyazaki T (1997) Development of KOH activated high surface area carbon and its application to drinking water purification. Carbon 35:1315–1319

Parolo ME, Savini MC, Vallés JM, Baschini MT, Avena MJ (2008) Tetracycline adsorption on montmorillonite: pH and ionic strength effects. Appl Clay Sci 40:179–186

Passuello A, Cadiach O, Perez Y, Schuhmacher M (2012) A spatial multicriteria decision making tool to define the best agricultural areas for sewage sludge amendment. Environ Int 38:1–9

Pils JRV, Laird DA (2007) Sorption of tetracycline and chlortetracycline on K- and Ca-saturated soil clays, humic substances, and clay humic complexes. Environ Sci Technol 41:1928–1933

Poling BE, Prausnitz JM, John Paul OC, Reid RC (2001) The properties of gases and liquids, vol 5. McGraw-Hill, New York

Radovic LR, Moreno-Castilla C, Rivera-Utrilla J (2001) Carbon materials as adsorbents in aqueous solutions. Chem Phys Carbon 27:227–405

Rivera-Utrilla J, Sánchez-Polo M (2002) The role of dispersive and electrostatic interactions in aqueous phase adsorption of naphthalenesulphonic acids on ozone-treated activated carbons. Carbon 40:2685–2269

Rivera-Utrilla J, Sánchez-Polo M (2004) Ozonation of naphthalenesulphonic acid in the aqueous phase in the presence of basic activated carbons. Langmuir 20(21):9217–9222

Rivera-Utrilla J, Bautista-Toledo I, Ferro-García MA, Moreno-Castilla C (2001) Activated carbon surface modifications by adsorption of bacteria and their effect on aqueous lead adsorption. J Chem Technol Biot 76:1209–1215

Rivera-Utrilla J, Bautista-Toledo I, Ferro-García MA, Moreno-Castilla C (2003) Bioadsorption of Pb(II), Cd(II), and Cr(VI) on activated carbon from aqueous solutions. Carbon 41:323–330

Rivera-Utrilla J, Prados-Joya G, Sánchez-Polo M, Ferro-García MA, Bautista-Toledo I (2009) Removal of nitroimidazole antibiotics from aqueous solution by adsorption/bioadsorption on activated carbón. J Hazard Mater 170:298–305

Rivera-Utrilla J, Sánchez-Polo M, Gómez-Serrano V, Álvarez PM, Alvim-Ferraz MCM, Dias JM (2011) Activated carbon modifications to enhance its water treatment applications, an overview. J Hazard Mater 187:1–23

Rivera-Utrilla J, Gómez-Pacheco CV, Sánchez-Polo M, López-Peñalver JJ, Ocampo-Pérez R (2013a) Tetracycline removal from water by adsorption/bioadsorption on activated carbons and sludge-derived adsorbents. J Environ Manag 131:16–24

Rivera-Utrilla J, Sánchez-Polo M, Ferro-García MA, Prados-Joya G, Ocampo-Pérez R (2013b) Pharmaceuticals as emerging contaminants and their removal from water. A review. Chemosphere 93:1268–1287

Rodriguez-Reinoso F, Linares-Solano A (1989) Microporous structure of activated carbons as revealed by adsorption methods. Chem Phys Carbon 21:1–146

Ros A, Lillo-Ródenas MA, Fuente E, Montes-Morán MA, Martín MJ, Linares-Solano A (2006) High surface area materials prepared from sewage sludge-based precursors. Chemosphere 65:132–140

Sánchez-Polo M, Rivera-Utrilla J (2003) Effect of the ozone–carbon reaction on the catalytic activity of activated carbon during the degradation of 1, 3, 6-naphthalenetrisulphonic acid with ozone. Carbon 41(2):303–307

Sánchez-Polo M, Rivera-Utrilla J (2006) Ozonation of naphthalenetrisulphonic acid in the presence of activated carbons prepared from petroleum coke. Appl Catal B-Environ 67:113–120

Shao L, Ren Z, Zhang G, Chen L (2012) Facile synthesis, characterization of a $MnFe_2O_4$/activated carbon magnetic composite and its effectiveness in tetracycline removal. Mater Chem Phys 135:16–24

Sheng GP, Yu HQ, Yu Z (2005) Extraction of extracellular polymeric substances from the photosynthetic bacterium Rhodopseudomonas acidophila. Appl Microbiol Biot 67:125–130

Simazaki D, Fujiwara J, Manabe S, Matsuda M, Asami M, Kunikane S (2008) Removal of selected pharmaceuticals by chlorination, coagulation-sedimentation and powdered activated carbon treatment. Water Sci Technol 58:1129–1135

Snyder SA, Adham S, Redding AM, Cannon FS, DeCarolis J, Oppenheimer J (2007) Role of membranes and activated carbon in the removal of endocrine disruptors and pharmaceuticals. Desalination 202:156–181

Srivastava VC, Mall ID, Mishra IM (2006) Equilibrium modelling of single and binary adsorption of cadmium and nickel onto bagasse fly ash. Chem Eng J 117:79–91

Stackelberg PE, Gibs J, Furlong ET, Meyer MT, Zaugg SD, Lippincott RL (2007) Efficiency of conventional drinking-water-treatment processes in removal of pharmaceuticals and other organic compounds. Sci Total Environ 377:255–272

Tally FP, Goldin B, Sullivan NE (1981) Nitroimidazoles: in vitro activity and efficacy in anaerobic infections. Scand J Infect Dis 13:46–53

Ternes TA, Meisenheimer M, McDowell D, Sacher F, Brauch HJ, Haist-Gulde B, Zulei-Seibert N (2002) Removal of pharmaceuticals during drinking water treatment. Environ Sci Technol 36:3855–3863

Traegner UK, Suidan MT (1989) Parameter evaluation for carbon adsorption. J Env Eng Div-ASCE (J Environ Eng-ASCE) 115:109–128

Turku I, Sainio T, Paatero E (2007) Thermodynamics of tetracycline adsorption on silica. Environ Chem Lett 5:225–228

USEPA (1991) Granular activated carbon treatment report EPA-540/2–91/024. US Environmental Protection Agency, US Government Printing Office, Washington, DC

Van der Bijl P, Pitigoi-Aron G (1995) Tetracyclines and calcified tissues. Ann Dent 54:69–72

Vidal CB, Seredych M, Rodríguez-Castellón E, Nascimento RF, Bandosz TJ (2015) Effect of nanoporous carbon surface chemistry on the removal of endocrine disruptors from water phase. J Colloid Interf Sci 449:180–191

Wang R, Wei RC, Liu T, Wang T (2008a) Sorption characteristics of veterinary antibiotics chlortetracycline on manure. Huan Jing Ke Xue 29:1363–1368

Wang X, Zhu N, Yin B (2008b) Preparation of sludge-based activated carbon and its application in dye wastewater treatment. J Hazard Mater 153:22–27

Wang YJ, Sun RJ, Xiao AY, Wang SQ, Zhou DM (2010) Phosphate affects the adsorption of tetracycline on two soils with different characteristics. Geoderma 156:237–242

Wang H, Wu X, Liu X, Cong P (2011) Application study of a modified phenolic resin as binder for hybrid fibers reinforced brake pad for railroad passenger-coach braking. J Macromol Sci Chem 48:261–270

Werther J, Ogada T (1999) Sewage sludge combustion. Prog Energ Combust 25:55–116

West CC, Harwell JH (1992) Surfactants and subsurface remediation. Environ Sci Technol 26:2324–2330

Wilke CR, Chang P (1955) Correlation of diffusion coefficients in dilute solutions. AIChE J 1(2):264–270

Yang S, Cha J, Carlson K (2005) Simultaneous extraction and analysis of 11 tetracycline and sulfonamide antibiotics in influent and effluent domestic wastewater by solid-phase extraction

and liquid chromatography-electrospray ionization tandem mass spectrometry. J Chromatogr A 1097:40–53

Yu Z, Peldszus S, Huck P-M (2008) Adsorption characteristics of selected pharmaceuticals and an endocrine disrupting compound-naproxen, carbamazepine and nonylphenol-on activated carbon. Water Res 42:2873–2882

Zhang L, Song X, Liu X, Yang L, Pan F, Lv J (2011) Studies on the removal of tetracycline by multi-walled carbon nanotubes. Chem Eng J 178:26–33

Zhou Q, Li Z, Shuang C, Li A, Zhang M, Wang M (2012) Efficient removal of tetracycline by reusable magnetic microspheres with a high surface area. Chem Eng J 210:350–356

Zhu X, Tsang DC, Chen F, Li S, Yang X (2015) Ciprofloxacin adsorption on graphene and granular activated carbon: kinetics, isotherms, and effects of solution chemistry. Environ Technol 36:3094–3102

Zielke U, Hüttinger KJ, Hoffman WP (1996) Surface-oxidized carbon fibers: I Surface structure and chemistry. Carbon 34:983–998

Zogorski JS, Faust SD (1977) Operational parameters for optimum removal of phenolic compounds from polluted waters by columns of activated carbon. AIChe Symp Ser 73:54–65

Zou YL, Huang H, Chu M, Lin JW, Yin DQ, Li YN (2012) Adsorption research of tetracycline from water by HCl-modified zeolite. Adv Mater Res 573:43–47